Available online at www.sciencedirect.com
ScienceDirect
Precambrian Research 163 (2008) 351–383
Precambrian Research
www.elsevier.com/locate/precamres

Rift melting of juvenile arc-derived crust: Geochemical evidence from Neoproterozoic volcanic and granitic rocks in the Jiangnan Orogen, South China

Yong-Fei Zheng [a,*], Rong-Xin Wu [a,d], Yuan-Bao Wu [a], Shao-Bing Zhang [a], Honglin Yuan [b], Fu-Yuan Wu [c]

[a] *CAS Key Laboratory of Crust-Mantle Materials and Environments, School of Earth and Space Sciences, University of Science and Technology of China, Hefei 230026, China*
[b] *State Key Laboratory of Continental Dynamics, Department of Geology, Northwest University, Xi'an 710069, China*
[c] *State Key Laboratory of Lithosphere Evolution, Institute of Geology and Geophysics, Chinese Academy of Sciences, Beijing 100029, China*
[d] *Department of Resource and Environmental Engineering, Anhui University of Science and Technology, Huainan 232001, China*

Received 4 October 2007; received in revised form 8 January 2008; accepted 28 January 2008

Abstract

A combined study of zircon U–Pb and Lu–Hf isotopes, mineral O isotopes, whole-rock elements and Sr–Nd isotopes was carried out for Neoproterozoic volcanics and granites from the eastern part of the Jiangnan Orogen in South China. The results are used to test controversial models of petrogenesis (plume-rift, slab-arc and plate-rift) for similar ages of magmatic rocks in South China. Zircon U–Pb dating yields two groups of ages at ~780 and ~825 Ma, respectively, corresponding to syn-rift and pre-rift magmatic events in response to supercontinental rifting. Both volcanic and granitic rocks show trace element features similar to those of arc-derived igneous rocks, but with more significant enrichment in large ion lithospheric elements relative to oceanic arc basalts. They have positive $\varepsilon_{Hf}(t)$ values of 3.6–6.3 for zircons, with Hf model ages of 1.12–1.21 Ga. This indicates reworking of late Mesoproterozoic juvenile crust for the origin of the Neoproterozoic magmatic rocks. Thus, oceanic arc magmatism would occur in the late Mesoproterozoic, with remarkable production of juvenile crust at the southeastern margin of the Yangtze Block. Because of the tectonic collapse of arc–continent collision orogen in the pre-rift stage, S-type magmatic rocks were generated by burial and anatexis of juvenile arc-derived crust to form the pre-rift episode of granodiorites and volcanics. In the syn-rift stage, the volcanics formed by reworking of arc-derived sedimentary rocks whereas the granite was generated by melting of the pre-rift igneous rocks. Emplacement of evolved felsic magmas along the rift tectonic zone would cause subsolidus high-T meteoric-hydrothermal alteration, resulting in varying $\delta^{18}O$ values for minerals from the volcanic and granitic rocks. Therefore, the plate-rift model is advanced to account for petrogenesis of all Neoproterozoic magmatic rocks in South China, with lithospheric extsension as the driving force of supercontinental rifting. Partial melting due to arc-continent collision, orogenic collapse and supercontinental rifting is also proposed as a mechanism for the chemical differentiation of continental crust towards the felsic composition.

Keywords: Neoproterozoic magmatism; Continental accretion; Arc–continent collision; Orogenic collapse; Rift anatexis; Hydrothermal alteration

1. Introduction

With the advance of studies concerning assembly and breakup of the supercontinent Rodinia and the proposition of mantle superplume beneath South China (Li et al., 1995, 1999, 2003a,b), Neoproterozoic magmatic rocks in South China has lately become one of the important targets. Geochronological studies show widespread presence of Neoproterozoic magmatic rocks, mostly with ages of 830–740 Ma (e.g., Li et al., 2003a, 2005, 2008; Zheng et al., 2004, 2006; Zhou et al., 2006a,b; Zhu et al., 2006; Wu et al., 2007; Tang et al., 2008; Wang et al., 2008). With respect to their petrogenesis, however, it has been a hotly debated issue, with three models proposed: (1) plume-rift model (Li et al., 1999, 2003a,b, 2006), (2) slab-arc model (Zhou et al., 2002a, 2002b; Wang et al., 2004a), and (3) plate-rift model (Zheng et al., 2007a). Test of these models requires an integrated

* Corresponding author. Tel.: +86 551 3603554; fax: +86 551 3603554.
E-mail address: yfzheng@ustc.edu.cn (Y.-F. Zheng).

0301-9268/$ – see front matter © 2008 Elsevier B.V. All rights reserved.
doi:10.1016/j.precamres.2008.01.004

study of tectonics, petrology, geochronology and geochemistry to resolve when and how the subduction of oceanic crust, island-arc magmatism, slab melting, arc–continent collision, orogenic collapse, and rift magmatism occurred subsequentially in association with the assembly and breakup of the supercontinent Rodinia in South China. In particular, contemporaneous growth of juvenile crust is implicated in the plume-rift and slab-arc models, whereas Zr saturation is required for the formation of igneous zircons in the juvenile crust comprised of plume or arc magmatic rocks. Thus, the presence or absence of mid-Neoproterozoic juvenile crust is a threshold to prove or disprove the two models. This can be tested by the zircon Hf model age because it has been demonstrated to be a close proxy for timing of juvenile crust growth (e.g., Kemp et al., 2006; Zhang et al., 2006; Zheng et al., 2006, 2007a).

On the other hand, metaigneous rocks in the Dabie–Sulu orogenic belt, the northern margin of South China, have protolith ages of 740–780 Ma and negative O isotope anomalies (Zheng et al., 2003, 2004, 2006, 2007b; Wu et al., 2007; Tang et al., 2008). It is demonstrated that these igneous rocks are petrogenetically related to the Rodinia breakup and associated high-T meteoric-hydrothermal alteration in rift tectonic zones. The O isotope record of surface water–rock interaction is also found in contemporaneous magmatic rocks at the western margin of South China (Zheng et al., 2007a). It appears that rift tectonic zones are a favorable place for high-T meteoric-hydrothermal alteration and low $\delta^{18}O$ magmatism (e.g., Taylor, 1977; Bindeman and Valley, 2001; Zheng et al., 2004; Wu et al., 2007). Growth and reworking of juvenile crust are indicated by the Lu–Hf isotope composition of zircon from the two occurrences of the Dabie–Sulu Orogen (Zheng et al., 2006, 2007a; Chen et al., 2007a). It is intriguing whether the O and Hf isotope features also occur in the interior of South China, particular in the Jiangnan Orogen that marks the convergence between the Yangtze Block and the Cathaysia Block.

Li et al. (2003a) demonstrated two major phases of widespread magmatism in South China during the Neoproterozoic: the first one, at ca. 830–795 Ma, started before the continental rift but continued into the first stage of the rifting; the second one, ca. 780–745 Ma, occurred during the peak stage of the rifting. Reworking of juvenile crust was found in ~825 Ma granodiorite in the eastern part of the Jiangnan Orogen (Wu et al., 2006a). This region is a rift tectonic zone during the mid-Neoproterozoic (Wang and Li, 2003), with occurrence of granodiorites, granites and volcanics. Thus, it is interesting to see whether low $\delta^{18}O$ and positive $\varepsilon_{Hf}(t)$ features also occur in the second phase of magmatic rocks. This paper presents a combined study of zircon U–Pb and Lu–Hf isotopes, whole-rock elements and Sr–Nd isotopes, and mineral O isotopes for the granites and volcanics in the eastern part of the Jiangnan Orogen. The results provide insight into juvenile crust reworking and high-T hydrothermal alteration in association with rift magmatism. Furthermore, the three models of petrogenesis are tested against all of geological and geochemical observations available from Neoproterozoic igneous rocks in South China. The plate-rift model is thus advanced to interpret the all observations with consistent results for the same subjects.

2. Geological setting and samples

The Jiangnan Orogen is a Neoproterozoic orogen between the Yangtze and Cathaysia Blocks in South China (insert in Fig. 1). It is assumed to record continent–arc–continent collision in the early Neoproterozoic following the Grenvillian subduction of oceanic crust in the late Mesoproterozoic (Charvet et al., 1996; Li and Li, 2003; Wu et al., 2006a; Zheng et al., 2007a). About 740–830 Ma granitoids are common along this orogen (Li et al., 2003a,b, 2005, 2008; Wang et al., 2006, 2008; Wu et al., 2006a; Zhou et al., 2007a). Granites and volcanics in question are located in the eastern part of the Jiangnan Orogen. Geographically, they are located in the boundary between Anhui, Jiangxi and Zhenjiang provinces (Fig. 1).

The granites occur as a batholith in the Shi'ershan area, with a total outcrop area of about 500 km^2. The oldest country rocks are Mesoproterozoic to early Neoproterozoic low-grade metasediments, which are named as the Shangxi Group in South Anhui, the Shuangxiwu Group in Northwest Zhejiang and the Shuangqiaoshan Group in Northeast Jiangxi. The youngest country rocks are middle Neoproterozoic volcanosedimentary rocks, including the Jingtan Formation in South Anhui, the Shangshu Formation in Northwest Zhejiang and Northeast Jiangxi, which are ascribed to the Neoproterozoic rifting Formations in South China (Wang and Li, 2003). The volcanics of interest just belong to the Jingtan volcanosedimentary Formation in this area. They were dated to have a Sm–Nd isochron age of 829 ± 35 Ma (Xu et al., 1992). Since this age has a low precision, a credible formation age still needs to be resolved. Petrogenetic relationship between the Jingtan volcanics and the Shi'ershan granites is also an important issue to be studied.

The granitic batholith at Shi'ershan can be subdivided into many plutons, with relatively early or late intrusive relationships between them (Tang et al., 1997; Liu, 1997). The predominant rocks are K-feldspar granites; minor rhyolitic porphyrys and granodiorites were also observed in some areas. In general, the batholith has porphyritic to porphyroid textures, indicating its shallow emplacement. Major minerals include 20–35% quartz, 50–60% K-feldspar, 5–20% plagioclase, minor biotite and muscovite; accessory minerals include zircon, magnetite, epidote, pyroxene and so on.

Tang et al. (1997) reported TIMS zircon U–Pb ages of 765 ± 49 and 825 ± 3 Ma for the Shi'ershan granite. Liu (1997) reported TIMS zircon U–Pb ages of 761–765 Ma for this granite (no error was given), and interpreted it as S-type granite derived from supracrustal materials in the collisional orogen between the Yangtze Block and the Cathaysia Block. However, Li et al. (2003a) obtained a SHRIMP zircon U–Pb age of 779 ± 11 Ma for the granite and interpreted it as a product of syn-rift magmatism due to a mantle superplume event. An old U–Pb age of 854 ± 14 Ma was obtained for an inherited zircon (Li et al., 2003a). Although the zircon U–Pb ages of 760–780 Ma have been widely accepted as the emplacement ages of the granite, the geological significance for the old ages of 820–854 Ma still remains unclear.

Sixteen granite samples from the Shi'ershan batholith are used in this study. Samples 03WN60-64 were collected from the

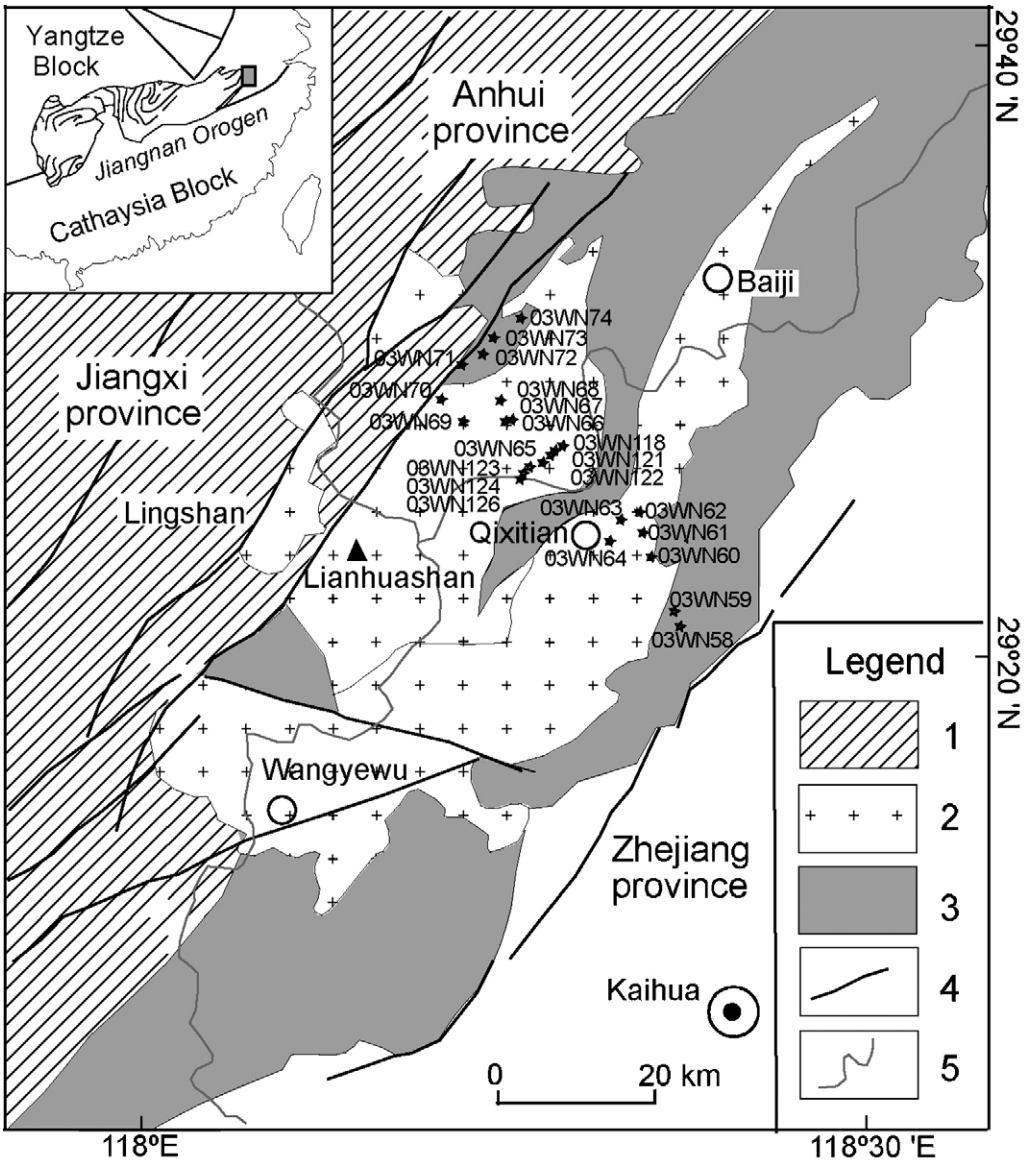

Fig. 1. Simplified geological map for Neoproterozoic magmatic rocks in the eastern part of the Jiangnan Orogen between the Yangtze and Cathaysia Blocks, South China. Geographically, they are located in the boundary between Anhui, Jiangxi and Zhenjiang provinces. Filled asterisks with numbers denote the sampling localities. Legend: (1) Mesoproterozoic to early Neoproterozoic metasediments; (2) Neoproterozoic granite; (3) Neoproterozoic volcanic to sedimentary rocks; (4) fault; (5) boundary between provinces.

Qixitian pluton; samples 03WN65-70 and samples 05WN118-126 were collected from the Lianhuashan pluton (Fig. 1). All the 16 samples were analysed for mineral O isotopes, six of which were selected for the analyses of whole-rock major and trace elements, Sm–Nd and Rb–Sr isotopes, and three of which were further selected for a combined study of zircon U–Pb dating. The three samples selected for the U–Pb dating include sample 03WN61 from the Qixitian pluton (29°23′58″N, 118°22′8″E) and samples 03WN65 (29°52′53″N, 118°28′59″E), 03WN68 (29°55′31″N, 118°33′19″E) from the Lianhuashan pluton.

Six volcanic samples from the periphery of the granite batholith are analysed in this study (Fig. 1). Field observations show that the granites are in contact to the volcanics. Samples 03WN58 and 03WN59 are tuff, collected from the eastern side of the batholith; samples 03WN71 to 03WN74 are dacite from the northwestern side. Both tuff and dacite contain mineral phenocrysts of quartz, K-feldspar and plagioclase. Pyroxene occurs in one sample of tuff (03WN58). All the six samples were analysed for mineral O isotopes, three of which were selected for zircon U–Pb dating, whole-rock major and trace elements, Sm–Nd and Rb–Sr isotopes. The three dated samples are 03WN58 from the Xiashan town, Kaihua county, Zhejiang province (29°23′58″N, 118°22′8″E), 03WN71 (29°29′26″N, 118°13′56″E) and 03WN73 (29°30′24″N, 118°14′27″E) from Longtian town, Xiuning county, Anhui province.

3. Analytical methods

After crushing, whole-rock samples were processed by conventional magnetic and density techniques to separate zircons

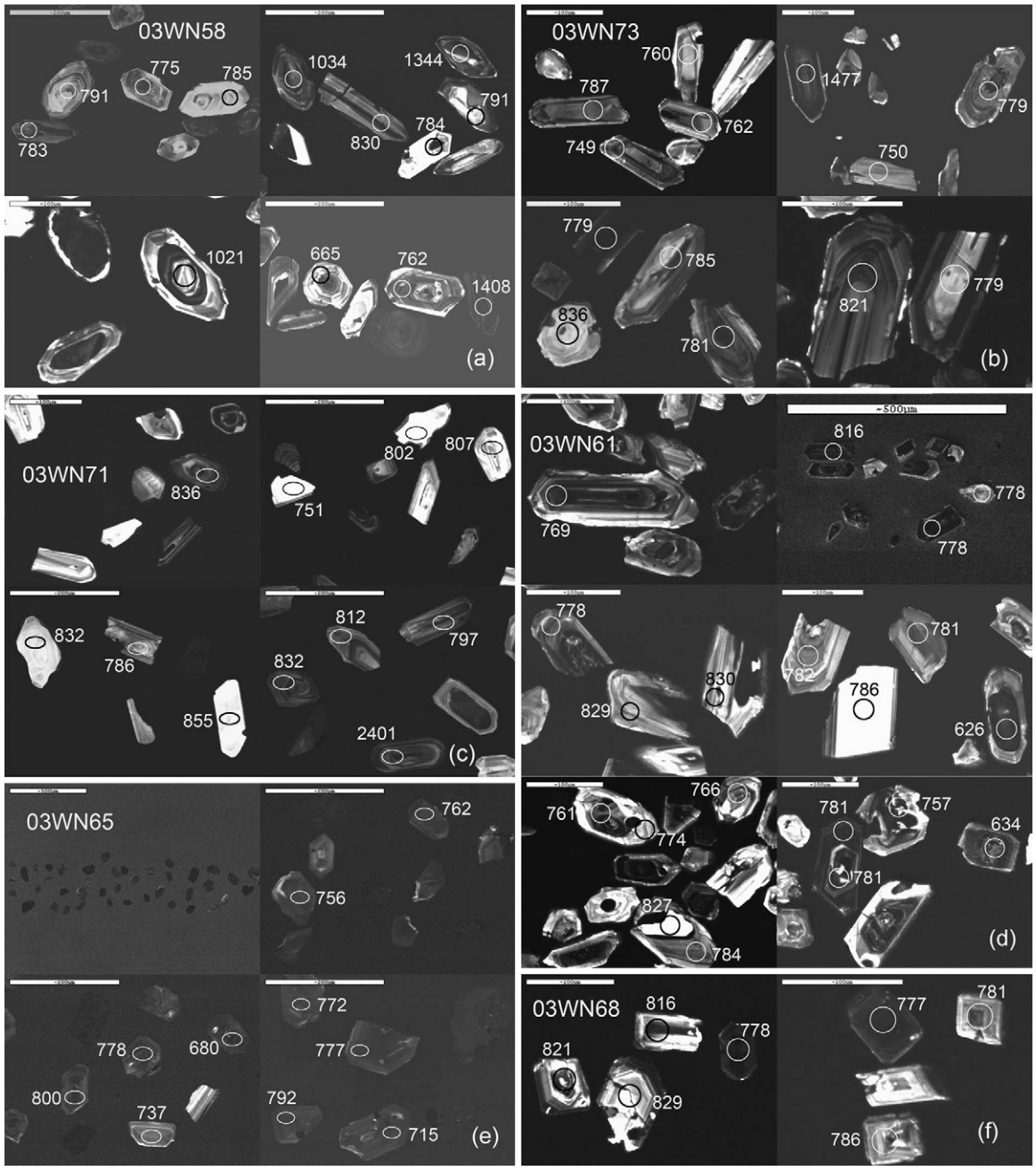

Fig. 2. CL images and U–Pb ages for zircons from Neoproterozoic magmatic rocks in the eastern part of the Jiangnan Orogen.

and other minerals. Selection of zircons was performed by hand-picking under a binocular microscope. The zircons were cast in an epoxy mount, which was then polished to section the crystals for analysis. CL imaging was taken using a JXA-8800R electron microprobe at the Institute of Mineral Resources in the Chinese Academy of Geological Sciences, Beijing. Both optical photomicrograph and CL image were taken as a guide to selection of U–Pb dating spot. Typical CL pictures are presented in Fig. 2, together with spot U–Pb ages. Morphology and internal structure of zircons are described and interpreted following the conventions of Corfu et al. (2003), Zheng et al. (2004) and Hoskin (2005). Together with their Th/U ratios, igneous zircons are classified into co-magmatically grown zircon and residual zircon (inherited from source rock), and hydrothermal zircons into hydrothermally altered zircon and hydrothermally grown zircon.

Zircon LA-ICPMS U–Pb dating was carried out at Northwest University in Xi'an. The GeoLas 200M laser-ablation system equipped with a 193 nm ArF-excimer laser was used in connection with ELAN6100 DRC ICP-MS. Helium was used as the carrier gas to enhance the transport efficiency of the ablated material. The detailed analytical method was described by Yuan et al. (2004). Spot diameter was 30 μm. Each complete analysis includes a background acquisition of about 30 s and a signal acquisition of about 80 s. The standard silicate glass NIST SRM610 was used to calculate U, Th and Pb concentrations.

Raw data were processed using GLITTER 4.0 software (Macquarie University). All measurements were performed using zircon 91,500 as the external standard with a recommended $^{206}Pb/^{238}U$ age of 1065.4 ± 0.6 Ma (Wiedenbeck et al., 1995). The common Pb correction was carried out by using the EXCEL program of ComPbCorr#_151 (Andersen, 2002). Ages were calculated using the ISOPLOT program of Ludwig (2001). The results are reported in 2σ errors.

Zircon SHRIMP U–Pb dating was carried out at Beijing SHRIMP Center in Chinese Academy of Geosciences, Beijing. The detailed analytical method was described by Williams (1998). The U–Pb isotope data were collected in sets of five scans throughout the masses and a reference zircon TEM (417 Ma) was analysed every fourth analysis. Common Pb was corrected using the measured ^{204}Pb. Common Pb isotope compositions for both the reference TEM and the samples are following the model of Stacey and Kramers (1975) at 417 Ma. The data were treated following the SQUID and the ISOPLOT program of Ludwig (2001). The results are reported in 2σ errors.

Zircon Lu–Hf isotopic analysis was carried out at the Institute of Geology and Geophysics in the Chinese Academy of Sciences, Beijing. Instrumental conditions and data acquisition were as described by Xu et al. (2004). A Geolas-193 laser-ablation microprobe was attached to a Neptune multi-collector ICPMS. Typical ablation time was about 30 s for 200 cycles, with a 10 Hz repetition rate, and a laser power of 100 mJ/pulse. A stationary spot was used for the present analyses, with a beam diameter of 63 μm (predominantly) or 31.5 μm. Ablation was conducted in He, this being combined with argon in a small mixing chamber prior to transport into the ICP torch. In the case of isotopic zoning or with intersecting cracks/inclusions, only the flattest, most stable portions of the time-resolved signal were selected for integration. Isobaric interference of ^{176}Lu on ^{176}Hf was corrected by measuring the intensity of the interference-free ^{175}Lu isotope and using a recommended $^{176}Lu/^{175}Lu$ ratio of 0.02655 (Machado and Simonetti, 2001) to calculate $^{176}Lu/^{177}Hf$ ratios. Correction for isobaric interference of ^{176}Yb on ^{176}Hf was performed in 'real time' as advocated by Woodhead et al. (2004) and developed by Iizuka and Hirata (2005). This involved measuring the interference-free ^{172}Yb and ^{173}Yb during the analysis, calculating mean β_{Yb} value from ^{172}Yb and ^{173}Yb and using a recommended $^{176}Yb/^{172}Yb$ ratio of 0.5886 (Chu et al., 2002) and mean β_{Yb} value to calculate $^{176}Yb/^{177}Hf$ ratios (Wu et al., 2006b). Zircon 91500 was used as the reference standard afterwards, with a recommended $^{176}Hf/^{177}Hf$ ratio of 0.282306 ± 10 (Woodhead et al., 2004). All the Lu–Hf isotope analysis results were reported with the error in 2σ of the mean. We have adopted a decay constant for ^{176}Lu of 1.865×10^{-11} year^{-1} (Scherer et al., 2001). Initial $^{176}Hf/^{177}Hf$ ratios $\varepsilon_{Hf}(t)$ were calculated with reference to the chondritic reservoir (CHUR) of Blichert-Toft and Albarede (1997) at the time of zircon growth from the magma. Single-stage Hf model age (T_{DM1}) is calculated relative to the depleted mantle with present-day $^{176}Hf/^{177}Hf = 0.28325$ and $^{176}Lu/^{177}Hf = 0.0384$ (Nowell et al., 1998; Griffin et al., 2000). Zircon Hf model ages are interpreted following the convention that adopts single-stage model (T_{DM1}) relative to the depleted mantle when $\varepsilon_{Hf}(t)$ values are positive, but two-stage model (T_{DM2}) relative to average continental crust when $\varepsilon_{Hf}(t)$ values are negative.

Whole-rock major and trace elements, and Sm–Nd and Rb–Sr isotopes were analysed at Guangzhou Institute of Geochemistry in Chinese Academy of Sciences, Guangzhou. Major element oxides were determined using a Varian Vista Pro ICP-AES. Trace elements were determined using a PerkinElmer Sciex ELAN 6000 ICP-MS. Analyses of USGS rock standards (BCR-2, BHVO-1 and AGV-1) indicate precision and accuracy better than 1% for major elements and 5% for trace elements and REE.

Whole-rock Nd–Sr isotopic compositions were determined using a Micromass IsoProbe multi-collector (MC-ICPMS). The detailed analytical method was described by Li et al. (2002a, 2003a). Measured $^{143}Nd/^{144}Nd$ ratios were normalized to $^{146}Nd/^{144}Nd = 0.7219$, and measured $^{87}Sr/^{86}Sr$ ratios were normalized to $^{86}Sr/^{88}Sr = 0.1194$. The results are reported in 2σ errors. Single-stage model ages (T_{DM1}) are calculated relative to the depleted mantle (DePaolo, 1988), and two-age model ages (T_{DM2}) are calculated relative to the average continental crust with a $^{147}Sm/^{144}Nd$ ratio of 0.118 (Jahn and Condie, 1995).

Mineral O isotope analysis was carried out by the laser fluorination technique using a 25 W MIR-10 CO_2 laser at University of Science and Technology of China in Hefei. O_2 was directly transferred to a Delta+ mass spectrometer for the measurement of O isotope ratios (Zheng et al., 2002). The O isotope data are reported as parts per thousand differences (‰) from the reference standard VSMOW in the $\delta^{18}O$ notation. Errors for repeat measurements of each standard on a given day were better than ±0.1‰ (1σ) for $\delta^{18}O$. Two reference minerals were used: $\delta^{18}O = 5.8‰$ for UWG-2 garnet (Valley et al., 1995), and $\delta^{18}O = 10.0‰$ for 91,500 zircon (Zheng et al., 2004). The results are reported in 2σ errors. Mineral-pair O isotopic temperatures are calculated using the fractionation curves of Zheng (1991, 1993a,b), assuming preservation of isotope equilibration at the scale of sample measurement. Judgment and interpretation of O isotope equilibrium or disequilibrium between coexisting minerals are based on measured fractionation values and resultant sequence of O isotope temperatures in combination with rates of O diffusion in concerned minerals and corresponding sequence of closure temperatures (Giletti, 1986; Zheng and Fu, 1998; Zhao et al., 2004; Chen et al., 2007b).

4. Results

4.1. Zircon U–Pb age

Zircons from three granites and three volcanics were dated with reference to their CL images (Tables 1 and 2). Some of the CL images are presented in Fig. 2, together with corresponding $^{206}Pb/^{238}U$ ages. For each group of U–Pb isotope data for single samples, a weighted mean of $^{206}Pb/^{238}U$ age was calculated by means of the ISOPLOT program of Ludwig (2001). The results are presented with 2σ errors in the Wetherill-type concordia diagram (Fig. 3).

Table 1
LA-ICPMS zircon U–Pb isotopic data for Neoproterozoic magmatic rocks in the Jiangnan Orogen

Spot	Element (ppm)			Th/U	Isotope rate					±1σ	Age (Ma)					
	Th	U	Pb		$^{207}Pb/^{206}Pb$	±1σ	$^{207}Pb/^{235}U$	±1σ	$^{206}Pb/^{238}U$		$^{207}Pb/^{206}Pb$	±1σ	$^{207}Pb/^{235}U$	±1σ	$^{206}Pb/^{238}U$	±1σ
03WN58 tuff																
1	148.5	315.2	50.26	0.47	0.07043	0.0011	1.35837	0.02199	0.13986	0.00167	941	16	871	9	844	9
2	37.6	55.6	8.51	0.68	0.06341	0.00274	1.12831	0.04793	0.12902	0.00203	722	63	767	23	782	12
3	224.8	512.4	99.17	0.44	0.07847	0.00112	1.85251	0.02782	0.1712	0.00204	1159	14	1064	10	1019	11
4	262.7	163.1	29.20	1.61	0.06797	0.00162	1.17822	0.02724	0.12573	0.00156	867	49	790	13	763	9
5	287.3	216.5	31.74	1.33	0.06637	0.00144	0.99465	0.02178	0.10868	0.00137	818	25	701	11	665	8
6	222.3	118.1	22.95	1.88	0.0646	0.00193	1.118	0.03313	0.1255	0.00171	761	40	762	16	762	10
7	375.4	346.9	109.98	1.08	0.1136	0.0016	3.82354	0.05645	0.24409	0.00295	1858	12	1598	12	1408	15
8	57.5	240.4	46.45	0.24	0.07939	0.00124	1.87928	0.03045	0.17168	0.00207	1182	15	1074	11	1021	11
9	233.3	131.9	27.59	1.77	0.07696	0.00158	1.46297	0.03018	0.13786	0.00174	1120	22	915	12	833	10
10	95.7	278.2	42.49	0.34	0.06632	0.00105	1.25912	0.02069	0.13769	0.00165	816	16	828	9	832	9
11	56.2	268.6	40.56	0.21	0.06972	0.00132	1.32147	0.02536	0.13747	0.00169	920	20	855	11	830	10
12	36.2	127.9	21.24	0.28	0.07061	0.00327	1.27141	0.05594	0.1306	0.00187	946	97	833	25	791	11
13	128.4	218.3	61.82	0.59	0.087	0.00127	2.78124	0.04219	0.23186	0.00278	1360	13	1351	11	1344	15
14	91.9	275.2	57.30	0.33	0.08598	0.00151	2.06255	0.03699	0.17399	0.00214	1338	17	1136	12	1034	12
15	233.4	147.8	27.79	1.58	0.06398	0.00178	1.14019	0.03156	0.12926	0.00172	741	36	773	15	784	10
16	82.6	60.2	11.06	1.37	0.05935	0.00225	1.06863	0.03998	0.13059	0.00186	580	56	738	20	791	11
17	96.7	251.0	37.33	0.39	0.06548	0.00206	1.16553	0.03353	0.12909	0.00164	790	68	785	16	783	9
18	206.9	127.9	26.06	1.62	0.068	0.00443	1.19711	0.07574	0.12768	0.00197	869	139	799	35	775	11
19	75.7	45.6	9.30	1.66	0.07953	0.003	1.4191	0.05255	0.12942	0.00197	1185	49	897	22	785	11
20	1616.5	670.1	90.44	2.41	0.06396	0.00128	0.70768	0.01426	0.08025	0.00099	740	23	543	8	498	6
03WN73 dacite																
1	100.4	203.9	29.93	0.49	0.06958	0.00232	1.23321	0.04058	0.12879	0.00185	916	44	816	18	781	11
2	117.8	143.6	24.08	0.82	0.06404	0.00242	1.1418	0.04276	0.12953	0.00181	743	55	773	20	785	10
3	56.1	63.8	11.02	0.88	0.06937	0.00467	1.32402	0.08601	0.13843	0.00271	910	139	856	32	836	15
4	72.1	328.7	46.64	0.22	0.07012	0.00121	1.24066	0.02178	0.12852	0.00157	932	18	819	10	779	9
5	156.9	337.7	51.89	0.46	0.06733	0.00122	1.19047	0.02199	0.12842	0.00157	848	20	796	10	779	9
6	49.0	156.3	22.83	0.31	0.07413	0.00279	1.27895	0.04475	0.12513	0.00172	1045	78	836	20	760	10
7	148.7	89.1	18.26	1.67	0.07918	0.00276	1.49241	0.05111	0.13687	0.002	1177	45	927	21	827	11
8	66.4	130.8	22.16	0.51	0.07615	0.00562	1.30904	0.09327	0.12468	0.00237	1099	152	850	41	757	14
9	82.1	128.8	24.03	0.64	0.07481	0.00437	1.34038	0.07541	0.12996	0.00206	1063	121	863	33	788	12
10	211.8	156.9	30.63	1.35	0.07619	0.00233	1.43672	0.04353	0.1369	0.00186	1100	39	904	18	827	11
11	101.3	229.8	40.55	0.44	0.06677	0.00301	1.24154	0.05236	0.13486	0.00186	831	94	820	24	816	11
12	120.5	152.0	25.34	0.79	0.07372	0.00337	1.30553	0.05666	0.12844	0.00185	1034	95	848	25	779	11
13	142.7	620.7	350.70	0.23	0.10056	0.00434	3.56968	0.16646	0.25745	0.00307	1634	80	1543	11	1477	16
14	621.5	437.3	78.99	1.42	0.06617	0.00157	1.17155	0.02847	0.12841	0.00156	812	50	787	10	779	9
15	38.5	114.3	17.32	0.34	0.07549	0.00396	1.28388	0.06436	0.12335	0.00191	1082	108	839	29	750	11
16	68.8	180.4	30.51	0.38	0.06438	0.00569	1.15284	0.09954	0.12988	0.00249	754	194	779	47	787	14
17	39.7	157.3	24.36	0.25	0.06903	0.00635	1.17274	0.10503	0.12322	0.00262	900	197	788	49	749	15
18	234.9	269.1	45.17	0.87	0.0822	0.00505	1.45094	0.08556	0.12802	0.00223	1250	124	910	35	777	13
19	77.6	84.3	14.30	0.92	0.07218	0.00537	1.24509	0.08994	0.1251	0.00223	991	156	821	41	760	13
20	66.2	125.8	20.28	0.53	0.07218	0.00472	1.29817	0.07679	0.12545	0.00194	1070	126	845	28	762	11

03WN61 granite																
1	120.4	101.9	22.50	1.18	0.07400	0.00300	1.40142	0.05563	0.13735	0.00191	1041	82	890	17	830	11
2	276.6	256.6	48.87	1.08	0.07034	0.00146	1.33171	0.02779	0.13732	0.00170	938	23	860	12	829	10
3	155.4	247.7	39.02	0.63	0.07847	0.00167	1.38772	0.02963	0.12827	0.00161	1159	23	884	13	778	9
4	1369.7	880.5	163.55	1.56	0.06646	0.00104	1.17543	0.01904	0.12828	0.00152	821	16	789	9	778	9
5	171.1	694.6	107.62	0.25	0.07797	0.00210	1.45081	0.03860	0.13495	0.00181	1146	32	910	16	816	10
6	157.0	372.4	56.08	0.42	0.07330	0.00160	1.28084	0.02791	0.12673	0.00160	1022	24	837	12	769	9
7	171.3	204.2	37.49	0.84	0.06980	0.00329	1.28412	0.05781	0.13343	0.00188	922	99	839	26	807	11
8	99.7	193.6	31.94	0.51	0.06691	0.00288	1.16335	0.04744	0.12610	0.00175	835	92	784	22	766	10
9	21.6	225.4	33.48	0.10	0.07317	0.00144	1.38010	0.02742	0.13680	0.00168	1019	21	880	12	827	10
10	94.1	282.4	39.97	0.33	0.06911	0.00148	1.23140	0.02640	0.12924	0.00161	902	24	815	12	784	9
11	82.9	158.9	24.52	0.52	0.05728	0.00243	1.00752	0.04249	0.12759	0.00175	502	69	708	21	774	10
12	220.4	344.3	55.45	0.64	0.06410	0.00267	1.10771	0.04361	0.12533	0.00168	745	90	757	21	761	10
13	355.6	489.0	85.03	0.73	0.06716	0.00258	1.17040	0.04236	0.12639	0.00165	843	82	787	20	767	9
14	309.5	876.5	103.95	0.35	0.06517	0.00096	0.92898	0.01426	0.10340	0.00121	780	15	667	8	634	7
15	1144.9	539.1	116.06	2.12	0.07068	0.00123	1.21394	0.02160	0.12458	0.00150	948	18	807	10	757	9
16	309.5	483.2	83.87	0.64	0.06913	0.00125	1.22679	0.02253	0.12872	0.00156	903	19	813	10	781	9
17	229.8	942.3	137.26	0.24	0.06413	0.00085	1.13949	0.01599	0.12888	0.00150	746	13	772	8	781	9
18	102.7	145.0	23.96	0.71	0.07928	0.00505	1.34433	0.08228	0.12299	0.00217	1179	130	865	36	748	12
19	627.1	1578.7	191.06	0.40	0.06226	0.00078	0.87482	0.01164	0.10192	0.00118	683	13	638	6	626	7
20	192.7	315.8	49.84	0.61	0.07097	0.00161	1.26047	0.02859	0.12883	0.00164	957	26	828	13	781	9
21	77.5	96.8	17.60	0.80	0.07991	0.00273	1.42828	0.04771	0.12966	0.00193	1195	42	901	20	786	11
22	124.4	201.5	32.58	0.62	0.06821	0.00139	1.21314	0.02493	0.12902	0.00160	875	23	807	11	782	9
23	505.5	959.8	150.80	0.53	0.06419	0.00082	1.14097	0.01541	0.12895	0.00150	748	13	773	7	782	9
24	251.0	257.6	47.43	0.97	0.07040	0.00167	1.30593	0.03091	0.13457	0.00174	940	28	848	14	814	10
25	115.7	141.0	24.27	0.82	0.07328	0.00168	1.30563	0.02988	0.12926	0.00166	1022	26	848	13	784	9
03WN68 granite																
1	206.7	274.1	55.91	0.75	0.06578	0.00423	1.14500	0.07147	0.12625	0.00193	799	139	775	34	766	11
2	319.1	454.6	73.83	0.70	0.06469	0.00239	1.13414	0.03918	0.12715	0.00168	764	80	770	19	772	10
3	241.5	348.1	55.43	0.69	0.07198	0.00121	1.27910	0.02220	0.12887	0.00160	985	17	836	10	781	9
4	741.2	982.0	157.85	0.75	0.06830	0.00090	1.20714	0.01696	0.12818	0.00154	878	13	804	8	777	9
5	241.8	349.5	62.83	0.69	0.06433	0.00141	1.14981	0.02614	0.12964	0.00161	752	46	777	10	786	9
6	640.0	904.3	142.07	0.71	0.07155	0.00118	1.26591	0.02161	0.12834	0.00159	973	17	831	10	778	9
7	312.3	389.9	70.50	0.80	0.07094	0.00281	1.31935	0.04896	0.13489	0.00185	956	83	854	21	816	11
8	133.9	244.3	40.26	0.55	0.06799	0.00135	1.28656	0.02610	0.13727	0.00175	868	22	840	12	829	10
9	337.8	417.2	76.39	0.81	0.06681	0.00281	1.25036	0.04889	0.13574	0.00184	832	88	824	22	821	10
10	263.5	382.9	63.70	0.69	0.06973	0.00295	1.22098	0.04863	0.12699	0.00179	920	89	810	22	771	10

Table 2
SHRIMP zircon U–Pb isotope data for Neoproterozoic magmatic rocks in the Jiangnan Orogen

Spot	Element (ppm)			Th/U	Isotope rate					±1σ	Age (Ma)			
	Th	U	Pb		$^{207}Pb/^{206}Pb$	±1σ	$^{207}Pb/^{235}U$	±1σ	$^{206}Pb/^{238}U$		$^{207}Pb/^{206}Pb$	±1σ	$^{206}Pb/^{238}U$	±1σ
03WN71 dacite														
1.1	620	396	47	1.62	0.0669	0.001004	1.277	0.04597	0.1384	0.00457	834	31	836	26
2.1	245	158	18	1.61	0.0603	0.002894	1.109	0.06543	0.1334	0.0044	614	100	807	25
3.1	90	75	9	1.25	0.06	0.00348	1.096	0.07453	0.1325	0.00451	602	130	802	26
4.1	70	66	7	1.10	0.0523	0.002877	0.89	0.05518	0.1235	0.00432	297	250	751	25
5.1	120	362	141	0.34	0.1764	0.003175	10.97	0.40589	0.451	0.01488	2619	30	2401	66
6.1	396	616	73	0.66	0.0661	0.000727	1.256	0.04396	0.1378	0.00455	810	23	832	26
7.1	300	294	34	1.05	0.0676	0.001149	1.25	0.04625	0.1342	0.00443	856	36	812	25
8.1	307	276	31	1.15	0.0656	0.001181	1.191	0.04526	0.1316	0.00434	795	37	797	25
9.1	37	61	7	0.62	0.0638	0.00319	1.212	0.07393	0.1378	0.00469	735	110	832	27
10.1	32	42	5	0.77	0.0665	0.003658	1.301	0.08066	0.1419	0.00568	822	250	855	32
11.1	196	148	17	1.37	0.0587	0.00317	1.049	0.06609	0.1298	0.00428	554	120	786	25
03WN65 granite														
1.1	897.0	1479.0	165.0	0.62	0.06533	0.00038	1.15400	0.03808	0.12810	0.00423	785	12	777	24
2.1	625.0	1006.0	113.0	0.64	0.06478	0.00053	1.16800	0.03971	0.13080	0.00432	767	17	792	24
3.1	574.0	1073.0	108.0	0.55	0.06545	0.00062	1.05900	0.03601	0.11730	0.00387	789	20	715	22
4.1	994.0	1476.0	168.0	0.70	0.06454	0.00039	1.17700	0.03884	0.13220	0.00436	759	13	800	25
5.1	193.0	438.0	45.6	0.46	0.06530	0.00091	1.09000	0.03924	0.12110	0.00400	784	29	737	23
6.1	672.0	1170.0	129.0	0.59	0.06540	0.00044	1.15700	0.03818	0.12830	0.00423	787	14	778	24
7.1	979.0	1655.0	159.0	0.61	0.06530	0.00176	1.00100	0.04204	0.11130	0.00367	783	57	680	21
8.1	535.0	875.0	94.4	0.63	0.06583	0.00051	1.13900	0.03873	0.12550	0.00414	801	16	762	24
9.1	431.0	733.0	78.6	0.61	0.06448	0.00090	1.10600	0.03982	0.12440	0.00411	757	23	756	23
10.1	779.0	1249.0	137.0	0.64	0.06547	0.00043	1.14800	0.03788	0.12710	0.00419	789	14	772	24

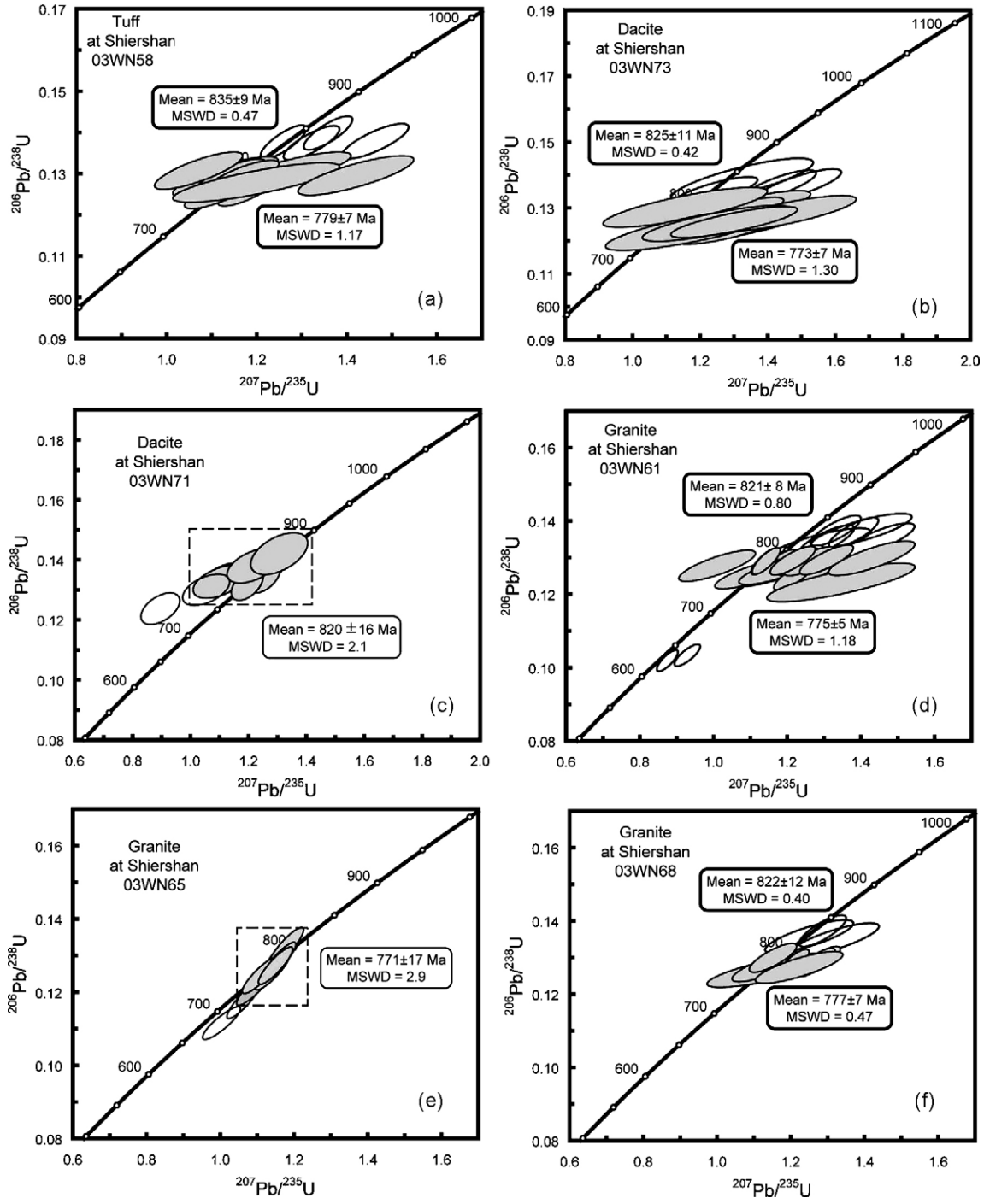

Fig. 3. U–Pb concordia diagram of zircons from Neoproterozoic magmatic rocks in the eastern part of the Jiangnan Orogen.

4.1.1. Volcanics

Zircons from tuff 03WN58 are euhedral, pale-yellowed and translucent. Most of them are equant to long prismatic. Crystal lengths range from 100 to 200 μm, with aspect ratios of 1:1–3:1. CL imaging reveals that most zircons are homogeneously oscillatory or planar zoned (Fig. 2a), and are interpreted as the result of magmatic growth. Some crystals exhibit structures of core-rim or core-mantle-rim. Twenty analyses were obtained by the LA-ICPMS method (Table 1). The sample has U contents from 45 to 670 ppm and Th from 36 to 1616 ppm, with Th/U ratios of 0.21–2.41 (Table 1). Spots #3, #7, #8, #13 and #14 are inherited domains of zircon as identified by their relatively dark CL images (Fig. 2a), yielding $^{206}Pb/^{238}U$ ages of older than 1000 Ma (Table 1). Spot #5 is partially recrystallized, with a young $^{206}Pb/^{238}U$ age of 665 ± 8 Ma. Spot #20 yields a $^{206}Pb/^{238}U$ age of 498 ± 6 Ma that is much younger than others (Table 1). Due to very high contents of U (670 ppm) and Th (1617 ppm), this young zircon is interpreted to experience metamictization resetting its U–Pb system. The other $^{206}Pb/^{238}U$ ages are subdivided into two groups, with weighted means at

779 ± 7 and 835 ± 9 Ma, respectively (Fig. 3a). As illustrated in Fig. 2a, about 779 Ma zircons are predominant, with medium CL brightness, clear oscillatory zoning, which are typical for magmatic zircons. Most of zircons with the ages older than 820 Ma are euhedral and magmatically zoned without apparent resorption in the CL images, thus they may be xenocrysts acquired during the magma emplacement.

Zircons from dacite 03WN73 are euhedral, pale-yellowed and translucent. Most of them are equant to long prismatic. Crystal lengths are about 100 μm, with aspect ratios of 1:1–3:1. Oscillatory zonings are common and clear in most crystals (Fig. 2b). Twenty U–Pb analyses were obtained by LA-ICPMS method (Table 1). The zircons have U contents from 63 to 620 ppm and Th from 38 to 621 ppm, with Th/U ratios of 0.22–1.67 (Table 1). Except for spot #13 that yields a $^{207}Pb/^{206}Pb$ age of 1634 ± 80 Ma and a $^{206}Pb/^{238}U$ age of 1477 ± 16 Ma (Table 1 and Fig. 2b), the other $^{206}Pb/^{238}U$ ages form two groups with weighted means at 773 ± 7 and 825 ± 11 Ma, respectively (Fig. 3b). From Th and U contents and Th/U ratios, there is no apparent discrimination between the two-age groups of zircon. The ages of ca. 773 Ma are predominant, representing the emplacement age. The older zircons are mostly euhedral and oscillatory zoned, probably xenocrysts.

Zircons from dacite 03WN71 are euhedral, pale-yellowed and translucent. Most of them are short to long prismatic. Crystal lengths are about 100 μm, with aspect ratios of 1.5:1–3:1. CL imaging reveals that most zircons are oscillatory or planar zoned (Fig. 2c). Some grains have core-rim structure. Some grains are bright in CL images, apparently are recrystallized. Some grains are rounded in rim, may be the results of resorption. Eleven U–b analyses were obtained by the SHRIMP method (Table 2). The zircons have U contents from 42 to 616 ppm and Th from 32 to 620 ppm, with Th/U ratios of 0.34–1.62 (Table 2). Spot #5.1 is a domain of an inherited zircon that is very euhedral and oscillatory zoned and yields a $^{207}Pb/^{206}Pb$ age of 2619 ± 30 Ma and a $^{206}Pb/^{238}U$ age of 2401 ± 66 Ma (Table 2 and Fig. 2c). Spot #4.1 is a domain of a recrystallized zircon that is very bright in CL images with low contents of U (66 ppm) and Th (70 ppm), and yields a $^{206}Pb/^{238}U$ age of 751 ± 25 Ma. Except for spots 4.1 and 11.1, the other $^{206}Pb/^{238}U$ ages are almost consistent with each other, defining a weighted mean of 820 ± 16 Ma, representing the emplacement age of dacite.

4.1.2. Granite

Zircons from granite 03WN61 at Qixitian are subhedral to euhedral, pale-yellowed and translucent. Most of them are equant to long prismatic. Crystal lengths range from 50 to 200 μm, with aspect ratios of 1:1–3:1. Magmatic oscillatory zonings are common in most crystals (Fig. 2d), but some are obscured. Some crystals exhibit core-rim structure. Rounded zircon cores can be observed within a few idiomorphic grains. Some zircons are partially resorbed and recrystallized with bright rounded rims, indicating they suffered post-magmatic high-*T* hydrothermal alteration. Twenty-five analyses were obtained by the LA-ICPMS method (Table 1). The results show U contents of 97–1579 ppm and Th of 21–1370 ppm, with Th/U ratios of 0.10–2.12 (Table 1). Spots #14 and #19 are dark and unzoned in their CL images (Fig. 2d), yielding $^{206}Pb/^{238}U$ ages of ca. 630 Ma that are much younger than the others (Table 1). The two spots also have very high contents of U (>800 ppm) and Th (>300 ppm) and thus they may be metamictized to reset their U–Pb systems and produce the younger ages. Spot 9#, a recrystallized and inherited core, unzoned with strong luminescence, shows clear resorption structures, yielding an old $^{206}Pb/^{238}U$ age of 827 ± 10 Ma (Fig. 2d). Spot 21# is also located in a recrystallized grain, giving a $^{206}Pb/^{238}U$ age of 786 ± 11 Ma. The $^{206}Pb/^{238}U$ ages are divided into two groups, with weighted means at 775 ± 5 and 821 ± 8 Ma, respectively (Fig. 3d). About 825 Ma zircons have rounded rims and obscured zonings, with one spot (#9) in the core, suggesting that they are of inherited origin. As illustrated in Fig. 2d, about 776 Ma zircons are predominant, some with medium CL brightness, clear oscillatory zoning, and relatively low contents of U and Th, which are typical magmatic zircons; whereas the others with dark CL and high contents of U and Th, which are similar to hydrothermally altered zircons as described by Hoskin (2005).

Zircons from granite 03WN65 at Lianhuashan are subhedral to euhedral, pale-yellowed to yellow. Most of them are equant to long prismatic. Crystal lengths range from 50 to 80 μm, with length to width ratios of 1:1–2:1. Most of them are dark and unzoned in CL images. Obscured oscillatory zonings can be observed in a few zircons (Fig. 2e). Ten analyses were obtained by the SHRIMP method (Table 2). The results show high U contents of 438–1655 ppm and Th of 193–994 ppm, with Th/U ratios of 0.46–0.70 (Table 2). Except for spots #3.1 and #7.1 that give younger ages of 715 and 680 Ma, the other $^{206}Pb/^{238}U$ ages are in agreement with each other and yield a weighted mean of 771 ± 17 Ma, interpreted as the crystallization age (Fig. 3e).

Zircons from granite 03WN68 at Lianhuashan are euhedral, pale-yellowed and translucent. They are equant to long prismatic. The lengths of these grains range from 50 to 100 μm, with length to width ratios of 1:1–2:1. Inherited zircon cores are observed within a few idiomorphic grains, partially resorbed and recrystallized with moderate CL brightness and obscured oscillatory zoning (Fig. 2f). Ten analyses were obtained by the LA-ICPMS method (Table 1). The results show U contents of 244–982 ppm and Th of 134–741 ppm, with Th/U ratios of 0.55–0.80 (Table 1). Spots #4 and #6 are dark and unzoned in CL images, with very high contents of U (982 and 904 ppm) and Th (741 and 640 ppm). $^{206}Pb/^{238}U$ ages form two groups with two weighted means at 777 ± 7 and 822 ± 12 Ma, respectively (Fig. 3f). The older spots are located in cores, with narrow rims of magmatic growth (Fig. 2f). Clearly, the value of 777 ± 7 Ma is the crystallization age. Some ~780 Ma zircons have moderate CL brightness, obscured magmatic zoning, and relatively low contents of U and Th, while the others are dark and unzoned, with high contents of U and Th (Fig. 2f and Table 1).

4.2. Major and trace elements

4.2.1. Volcanics

All volcanic samples at Jingtan are peraluminous, with high A/CNK ratios of 1.37–1.61 (Table 3). Tuff 03WN58 is plotted in the field of gabboic diorite (Fig. 4), corresponding to

Table 3
Major and trace element compositions of Neoproterozoic magmatic rocks

Sample	03WN58	03WN71	03WN73	03WN60	03WN61	03WN64	03WN65	03WN68	03WN70
	Tuff	Dacite	Dacite	Granite	Granite	Granite	Granite	Granite	Granite
Major element (%)									
SiO_2	54.88	70.60	70.83	78.53	69.34	76.02	78.39	77.88	78.60
TiO_2	0.86	0.77	0.44	0.22	0.28	0.21	0.08	0.10	0.07
Al_2O_3	15.93	14.32	14.57	11.80	12.25	12.52	12.15	11.59	11.73
$Fe_2O_3^T$	8.81	5.10	3.29	1.55	2.21	1.69	0.81	1.54	1.00
MnO	0.13	0.09	0.05	0.01	0.07	0.02	0.01	0.03	0.02
MgO	6.69	1.34	0.99	0.29	0.45	0.26	0.05	0.17	0.18
CaO	2.08	0.73	1.54	0.26	4.03	1.40	0.23	0.57	0.32
Na_2O	3.80	2.96	2.55	1.57	2.25	1.71	3.43	2.79	2.89
K_2O	0.86	2.53	3.37	4.28	4.05	4.74	4.87	4.44	4.44
P_2O_5	0.08	0.11	0.18	0.02	0.05	0.01	0.01	0.01	0.01
LOI	5.20	1.58	1.70	1.25	4.28	1.03	0.26	0.63	0.50
Total	99.32	100.11	99.51	99.78	99.26	99.61	100.3	99.75	99.76
A/CNK	1.45	1.61	1.37	1.53	0.79	1.19	1.07	1.11	1.16
Trace element (ppm)									
Mn	902	692	369	150	543	158	98.7	259	140
Ni	135	26.00	11.66	2.70	3.55	15.59	0.12	0.74	6.40
Ga	18.18	16.47	17.97	15.86	15.94	15.34	17.27	19.36	15.12
Rb	12.35	160	132	196	150	162	189	196	184
Ba	164	614	808	677	1804	849	424	710	533
Th	6.40	8.98	19.77	19.74	20.28	16.47	17.69	19.15	15.95
Nb	13.27	10.25	11.35	9.02	9.21	7.81	12.09	15.25	14.87
Ta	0.85	0.70	0.82	0.78	0.72	0.67	1.10	1.26	1.06
Hf	4.15	5.46	7.54	5.54	7.12	5.00	4.94	7.54	5.86
U	1.38	1.98	2.77	4.05	2.92	3.08	2.99	4.16	3.53
Sr	95.51	121	132	18.87	57.90	61.37	13.29	23.98	23.29
Zr	138	219	233	172	211	148	120	288	148
Y	25.48	28.19	35.09	38.33	43.32	41.96	73.09	71.46	78.27
La	23.96	33.71	45.78	29.50	49.93	32.03	38.86	48.60	39.95
Ce	46.17	67.43	96.74	62.86	98.86	67.91	82.80	98.19	86.65
Pr	5.65	8.31	12.22	7.96	11.77	8.31	11.44	13.14	10.97
Nd	20.76	31.05	47.26	30.80	43.05	29.31	44.25	51.49	42.45
Sm	4.22	5.95	9.40	6.74	8.47	6.32	10.79	11.86	9.73
Eu	0.93	1.44	1.45	0.64	1.01	0.67	0.62	1.07	0.68
Gd	3.53	5.25	7.76	6.77	7.68	5.94	12.07	12.97	10.29
Tb	0.65	0.85	1.19	1.24	1.25	1.10	2.10	2.28	1.94
Dy	4.02	4.94	6.28	7.12	7.22	6.56	12.98	12.68	11.26
Ho	0.82	1.02	1.14	1.47	1.43	1.32	2.73	2.85	2.33
Er	2.36	2.78	2.98	4.10	3.94	3.83	7.22	7.80	6.63
Tm	0.42	0.43	0.46	0.65	0.66	0.61	1.16	1.30	1.12
Yb	2.63	2.90	2.81	4.48	4.29	3.95	6.95	8.98	7.57
Lu	0.41	0.43	0.43	0.74	0.66	0.58	1.10	1.48	1.11
$(La/Yb)_N$	6.53	8.34	11.69	4.72	8.35	5.82	4.01	3.88	3.79
Eu/Eu*	0.72	0.77	0.50	0.29	0.38	0.33	0.17	0.26	0.21
T_{Zr} (°C)	765	840	835	835	780	800	760	855	800

basaltic andesite in volcanic termology. It has high contents of $Fe_2O_3^T$ (8.81%), MgO (6.69%), Na_2O (3.8%), and a low content of K_2O (0.86%). Dacites 03WN71 and 03WN73 are plotted in the field of dacite (Fig. 4). They have similar contents of K_2O (2.55 and 2.96%) and Na_2O (2.53 and 3.37%), relatively high mafic components ($TiO_2 + Fe_2O_3^T + MgO$) of 4.7 and 7.2%. Major elements such as TiO_2 and Al_2O_3 seem to have correlations with SiO_2 contents (Fig. 5), but only the three samples cannot tell much. All the samples have high LOI contents of 1.5–5.2%, suggesting secondary overprinting by various degrees of hydrothermal alteration.

The volcanics have similar REE partition patterns (Fig. 6a), with LREE enrichment and moderate negative Eu anomalies (Eu/Eu* = 0.52–0.79). They are interpreted as a result of fractional crystallization. In the primitive mantle-normalized spidergram (Fig. 6b), they are characterized by strong enrichment in large ion lithospheric elements (LILE) such as K, Rb, Ba, Th and U, but pronounced negative anomalies in Sr and high field elements (HFSE) such as Nb, Ta and Ti relative to neighbor elements. The dacite has REE and trace element patterns similar to the Neoproterozoic granodiorite in South Anhui, whereas tuff 03WN58 is close to the oceanic arc basalt.

According to the CL images and U–Pb dates (Fig. 2), the volcanics contains zircon xenocrysts, and only a few of them are partially resorbed. This indicates that the melt was saturated with zirconium when the old xenocrysts were incorporated. The

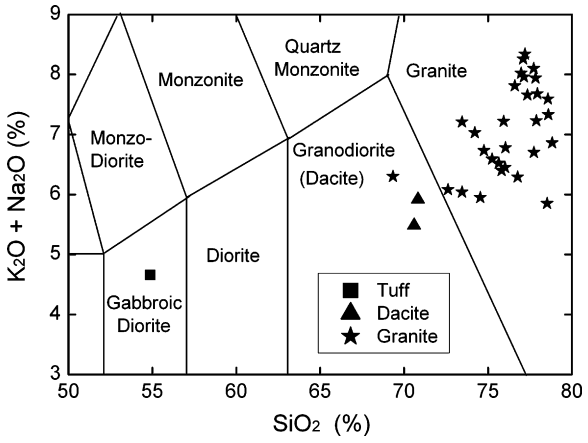

Fig. 4. TAS classification of Neoproterozoic magmatic rocks in the eastern part of the Jiangnan Orogen (the framework is after Middlemost, 1994).

measured Zr concentration and major element composition of whole-rock can be used to calculate the Zr saturation temperature (T_{Zr}). Following the calibration of Watson and Harrison (1983), the calculated T_{Zr} values are 766–841 °C (Table 3).

4.2.2. Granite

In the plot of silica versus alkali (Fig. 4), the Shi'ershan samples of granite fall within the granite field, except that sample 03WN61 lies in the granodiorite field (Fig. 4). Sample 03WN61 has a low A/CNK ratio of 0.79, mainly because of its CaO content of 4.03% greater than the others (0.04–1.40%). As a whole the granites have high contents of SiO_2 (74.7–78.5%), K_2O (3.99–5.64%), high K_2O/Na_2O ratios (1.5–3.0), high A/CNK ratios (1.1–1.6), and very low contents of 0.9–3.0% for mafic components ($TiO_2 + Fe_2O_3{}^T + MgO$). Major elements such as TiO_2 and Al_2O_3 are correlated with SiO_2 contents (Fig. 5). The samples from the Qixitian pluton have higher LOI contents of 1.0–4.3% than those of 0.26–0.63% for the Lianhuashan pluton (Table 3), indicating that they suffered different degrees of post-magmatic alteration.

All the samples have similar REE partition patterns showing LREE enrichment and strong Eu negative anomalies with Eu/Eu* ratios of 0.21–0.38 (Fig. 6c). In the primitive mantle-normalized spidergram, the granite shows strong enrichment in K, Rb, Ba, Th and U, but pronounced negative anomalies in Nb, Ta, Sr and Ti relative to the neighbor elements (Fig. 6d).

The CL imaging and U–Pb dating show that the granite contains the inherited zircons as cores or grains (Fig. 2d–f), indicating that Zr was saturated in the granitic melt. Therefore, the measured Zr concentration and whole-rock major element composition can be used to calculate the zircon saturation temperatures (T_{Zr}) for granitoids. Following the calibration of Watson and Harrison (1983), calculated T_{Zr} values are 760–855 °C (Table 3) with an average of 805 ± 19 °C.

4.3. Whole-rock Sr–Nd isotopes

4.3.1. Volcanics

The volcanics at Jingtan has Rb contents of 12.3–160.0 ppm and Sr contents of 95.5–131.9 ppm (Table 4), with $^{87}Rb/^{86}Sr$

Table 4
Whole-rock Rb–Sr and Sm-Nd isotope data for Neoproterozoic magmatic rocks in the Jiangnan Orogen

Sample	Age (Ma)	Sm (ppm)	Nd (ppm)	$^{147}Sm/^{144}Nd$	$^{143}Nd/^{144}Nd$ ($\pm 2\sigma_m$)	$\varepsilon_{Nd}(t)$	T_{DM1} (Ga)	T_{DM2} (Ga)	Rb (ppm)	Sr (ppm)	$^{87}Rb/^{86}Sr$	$^{87}Sr/^{86}Sr$ ($\pm 2\sigma_m$)	$I_{Sr}(t)$
Jingtan volcanics													
03WN58	776	4.218	20.76	0.1228	0.512167 ± 10	−1.87	1.65	1.60	12.35	95.51	0.373	0.718060 ± 13	0.713923
03WN71	820	5.95	31.05	0.1159	0.512061 ± 9	−2.79	1.69	1.71	160.0	121.0	3.821	0.726240 ± 12	0.681548
03WN73	776	9.398	47.26	0.1202	0.512161 ± 9	−1.71	1.61	1.59	131.8	131.9	2.891	0.740978 ± 13	0.708942
Shi'ershan granite													
03WN60	775	6.74	30.80	0.1322	0.512331 ± 9	0.44	1.53	1.42	196.4	18.87	30.453	0.855985 ± 15	0.516815
03WN61	775	8.47	43.05	0.1190	0.512277 ± 10	0.72	1.40	1.40	149.5	57.90	7.502	0.783363 ± 17	0.699810
03WN64	775	6.32	29.31	0.1304	0.512327 ± 9	0.55	1.50	1.41	162.4	61.37	7.687	0.781508 ± 16	0.695892
03WN65	775	10.79	44.25	0.1474	0.512329 ± 8	−1.13	1.88	1.54	188.7	13.29	41.632	0.877968 ± 61	0.416086
03WN68	775	11.86	51.49	0.1393	0.512317 ± 8	−0.53	1.70	1.50	196.2	23.98	24.039	0.899398 ± 16	0.631661
03WN70	775	9.73	42.45	0.1386	0.512339 ± 9	−0.04	1.64	1.46	183.5	23.29	23.179	0.912766 ± 16	0.654610

Note: The initial Nd and Sr isotope ratios were calculated either at $t = 825$ Ma or at $t = 780$ Ma after the U–Pb dating for the same samples.

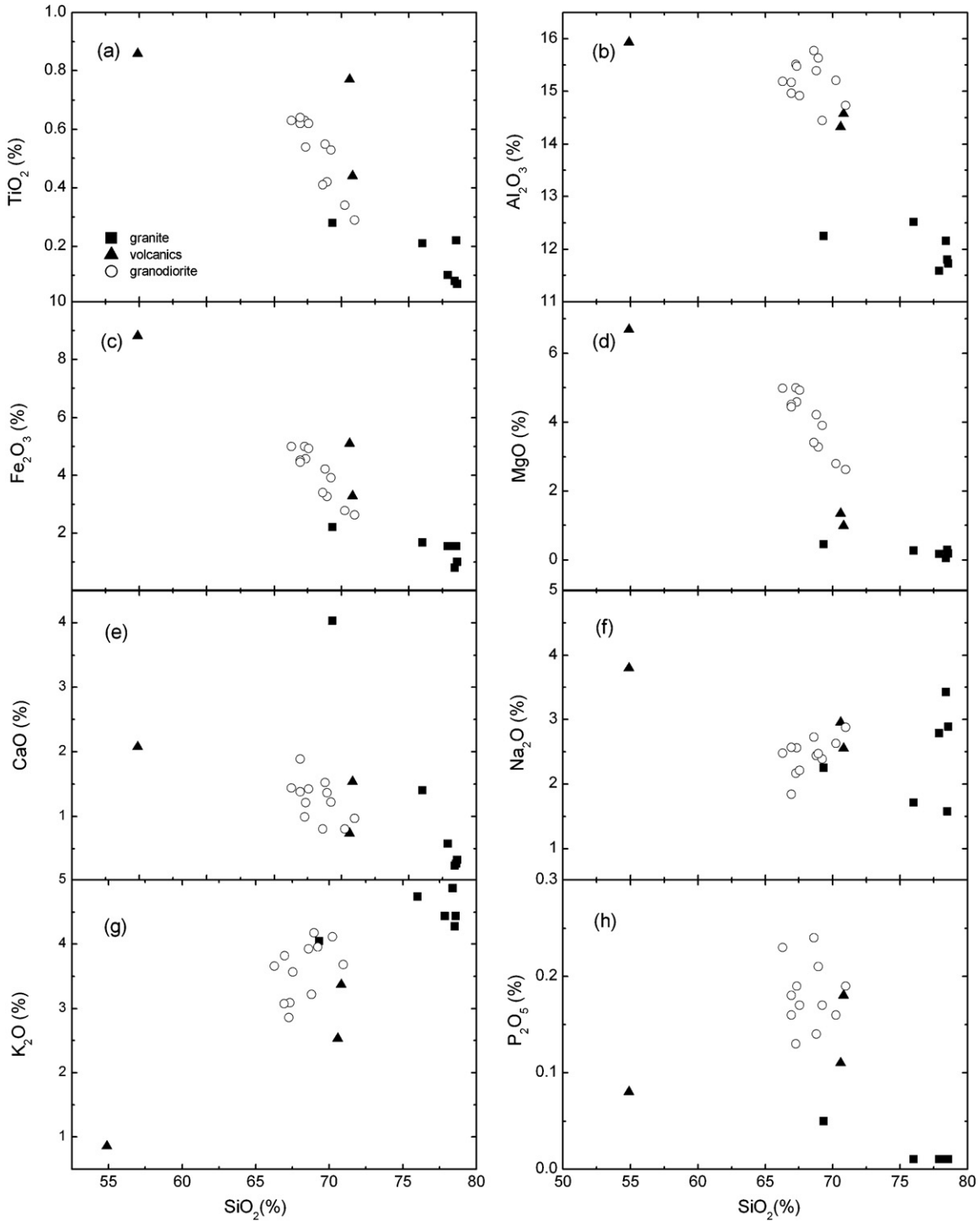

Fig. 5. Relationships diagram between major elements and SiO_2 contents for Neoproterozoic magmatic rocks in the eastern part of the Jiangnan Orogen.

ratios varying from 0.373 to 3.821. Calculated initial $^{87}Sr/^{86}Sr$ ratios range from 0.6815 to 0.7139, one of them lower than normal mantle ratios of 0.7035 (even the BABI value of 0.69897). This indicates that the dacitic magma was disturbed by hydrothermal alteration of externally derived fluids (Zheng, 1989). The volcanics has $^{147}Sm/^{144}Nd$ ratios of 0.1132–0.1514 and $^{143}Nd/^{144}Nd$ ratios of 0.512027–0.512298. Calculated $\varepsilon_{Nd}(t)$ values are −2.79 to −1.71 at their ages of magma emplacement, and corresponding single-stage Nd model ages (T_{DM1}) are 1.61–1.69 Ga.

4.3.2. Granite

The granite at Shi'ershan has Rb contents of 149.5–196.2 ppm and Sr contents of 13.29–61.37 ppm (Table 4), with $^{87}Rb/^{86}Sr$ ratios varying from 7.502 to 41.532. Calculated initial $^{87}Sr/^{86}Sr$ ratios at $t = 780$ Ma are 0.4161–0.6998, uni-

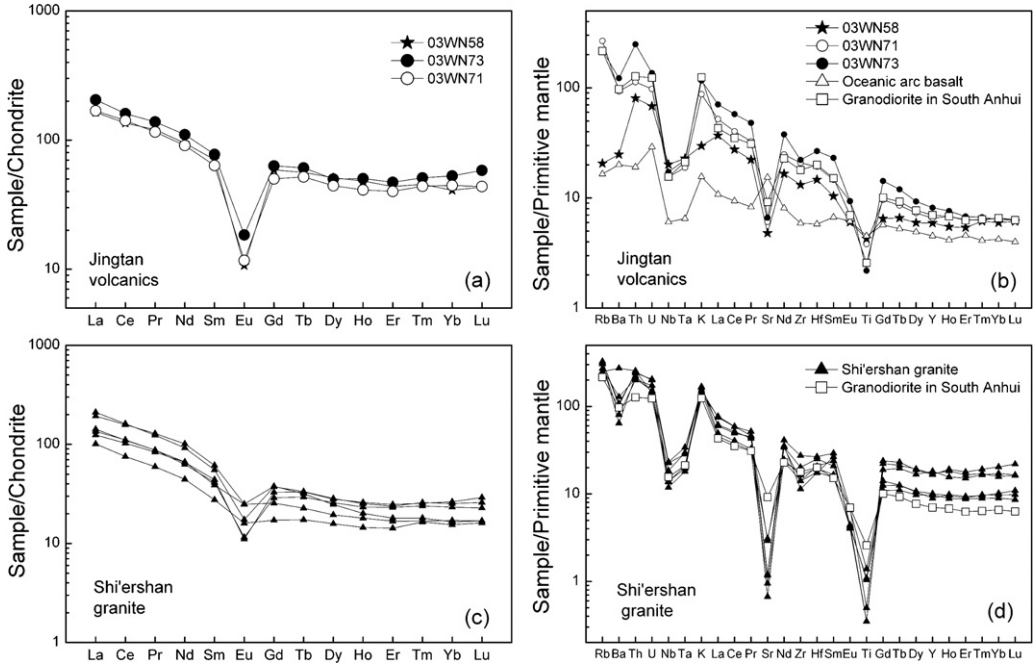

Fig. 6. Chondrite-normalized REE patterns and primitive mantle-normalized trace element spidergrams for Neoproterozoic magmatic rocks in the eastern part of the Jiangnan Orogen. Chondrite and primitive mantle values for normalization are from Sun and McDonough (1989) and McDonough and Sun (1995), respectively. Trace element concentrations of oceanic arc basalts are from Kelemen et al. (2004), and those of granodiorites in South Anhui from Wu et al. (2006a).

formly lower than the BABI value of 0.69897. Apparently, such unreasonably low initial $^{87}Sr/^{86}Sr$ ratios were caused by their high $^{87}Rb/^{86}Sr$ ratios of 7.5–41.6, because the Rb–Sr systems are easy to be disturbed by the hydrothermal alteration of externally derived fluids (Zheng, 1989). They have $^{147}Sm/^{144}Nd$ ratios of 0.119–0.147 and $^{143}Nd/^{144}Nd$ ratios of 0.512277–0.512339. Calculated $\varepsilon_{Nd}(t)$ values are −1.13 to 0.72 at $t = 780$ Ma, and corresponding to single-stage Nd model ages (T_{DM1}) of 1.40–1.88 Ga. Because the most $^{147}Sm/^{144}Nd$ ratios are greater than 0.13, calculated two-stage Nd model ages (T_{DM2}) cluster at 1.40–1.54 Ga.

4.4. Zircon Hf isotopes

The zircons from the four samples that were dated by U–Pb were also analysed for their Lu–Hf isotopes on domains of the same or similar structure, and the results are listed in Table 5. Initial $^{176}Hf/^{177}Hf$ ratios and $\varepsilon_{Hf}(t)$ values were calculated either at $t = 780$ Ma or at $t = 825$ Ma depending on their U–Pb ages (Fig. 3), which registered the timing of zircon growth from magmas. Figs. 7 and 8 show histograms of $\varepsilon_{Hf}(t)$ values and Hf model ages for the four samples, respectively.

4.4.1. Volcanics

Thirteen spots were analysed for zircon Lu–Hf isotopes in dacite 03WN71. Except for two negative $\varepsilon_{Hf}(t)$ values of −43.7 and −10.7 (spots #5 and #8 in Table 5), all other domains show positive $\varepsilon_{Hf}(t)$ values of 3.5 and 8.6 with a weighted mean of 4.7 ± 2.2 (Fig. 7a). Correspondingly, their Hf model ages are 1041–1310 Ma, with a weighted mean of 1.20 ± 0.09 Ga (Fig. 8a). The two negative $\varepsilon_{Hf}(t)$ spots have Hf model ages of 1.81 and 3.06 Ga; one of them is associated with the oldest U–Pb age of 2401 Ma. This indicates the presence of Paleoproterozoic and Archean crustal relicts in the source of Neoproterozoic volcanics.

Twenty spots were analysed for zircon Lu–Hf isotopes in dacite 03WN73. Except for a negative $\varepsilon_{Hf}(t)$ value, all other grains have $\varepsilon_{Hf}(t)$ values between 0.7 and 6.1 (Table 5), with a weighted mean of 3.6 ± 1.9 (Fig. 7b). Correspondingly, their Hf model ages are 1072–1316 Ma with a weighted mean of 1.21 ± 0.08 Ga (Fig. 8b). The negative $\varepsilon_{Hf}(t)$ value of −3.1 is associated with the oldest U–Pb age of 1477 Ma (spot #13 in Table 5). A two-stage Hf model age of 1.87 Ga can be calculated if a Lu/Hf ratio of 0.015 for average continental crust is used. This suggests incorporation of Paleoproterozoic crust relict into the source of Neoproterozoic volcanics.

4.4.2. Granite

Twenty-five spots were analysed for zircon Lu–Hf isotopes in granite 03WN61 from the Qitianxi pluton. Uniformly positive $\varepsilon_{Hf}(t)$ values scatter between 0.9 and 8.5 (Table 5), with a weighted mean of 4.5 ± 1.5 (Fig. 7c). Correspondingly, their Hf model ages are 1015–1326 Ma with a weighted mean of 1.18 ± 0.07 Ga (Fig. 8c).

Fifteen spots were analysed for zircon Lu–Hf isotopes in granite 03WN65 from the Lianhuashan pluton. Uniformly positive $\varepsilon_{Hf}(t)$ values cluster between 4.4 and 8.1 (Table 5), with a weighted mean of 6.3 ± 1.3 (Fig. 7d). Correspondingly, their Hf model ages are 1038–1195 Ma with a weighted mean of 1.12 ± 0.06 Ga (Fig. 8d).

Table 5
LA-MC-ICPMS zircon Lu–Hf isotope data for Neoproterozoic magmatic rocks in the Jiangnan Orogen

Spot no.	$^{176}Yb/^{177}Hf$	$^{176}Lu/^{177}Hf$	$^{176}Hf/^{177}Hf$	$\pm(2\sigma)$	U–Pb age (Ma)	$\varepsilon_{Hf}(t)$	$\pm(2\sigma)$	T_{DM} (Ma)	$\pm(2\sigma)$	Age spot
03WN71 dacite (t = 820 Ma)										
1	0.014180	0.000567	0.282393	0.000012	832	4.4	0.4	1202	34	9.1
2	0.069791	0.002475	0.282398	0.000016	786	3.5	0.6	1257	46	11.1
3	0.028840	0.001160	0.282520	0.000021	855	8.6	0.7	1041	58	10.1
5	0.042002	0.001567	0.282435	0.000014	832	5.3	0.5	1173	41	6.1
4	0.033963	0.001457	0.281980	0.000023		−10.7	0.8	1813	63	
6	0.062194	0.002594	0.282365	0.000023	797	2.3	0.8	1310	67	8.1
7	0.035667	0.001345	0.282365	0.000015	812	3.0	0.5	1266	41	7.1
8	0.019072	0.000760	0.281038	0.000018	2401	−43.7	0.6	3062	48	5.1
9	0.032467	0.001302	0.282444	0.000015		5.8	0.5	1153	43	
10	0.026154	0.001037	0.282396	0.000020	751	4.3	0.7	1211	55	4.1
11	0.027245	0.001055	0.282387	0.000025	807	3.9	0.9	1225	71	2.1
12	0.037954	0.001423	0.282415	0.000013	802	4.7	0.5	1198	38	3.1
13	0.044352	0.002010	0.282503	0.000019	836	7.5	0.7	1089	56	1.1
03WN73 dacite (t = 780 Ma)										
1	0.012450	0.000486	0.282453	0.000048	781	5.7	0.9	1115	66	1
2	0.024955	0.001050	0.282437	0.000057	785	4.8	1.0	1154	81	2
3	0.019668	0.000975	0.282349	0.000062	836	1.7	1.1	1276	87	3
4	0.011152	0.000412	0.282483	0.000043	779	6.8	0.8	1072	59	4
5	0.024147	0.001039	0.282365	0.000045	779	2.3	0.8	1256	63	5
6	0.011192	0.000431	0.282324	0.000049	760	1.1	0.9	1292	67	6
7	0.036099	0.001550	0.282419	0.000044	827	3.9	0.8	1195	63	7
8	0.014097	0.000633	0.282466	0.000071	757	6.1	1.3	1101	98	8
9	0.018048	0.000753	0.282379	0.000040	788	2.9	0.7	1226	56	9
10	0.013801	0.000567	0.282335	0.000068	827	1.5	1.2	1281	94	10
11	0.018280	0.000824	0.282316	0.000035	816	0.7	0.6	1316	48	11
12	0.031240	0.001326	0.282412	0.000050	779	3.8	0.9	1199	71	12
13	0.045302	0.001972	0.282227	0.000074	1477	−3.1	1.3	1485	106	13
14	0.025859	0.001068	0.282449	0.000040	779	5.2	0.7	1139	56	14
15	0.011810	0.000486	0.282448	0.000068	750	5.5	1.2	1123	94	15
16	0.011084	0.000427	0.282458	0.000090	787	5.9	1.6	1107	125	16
17	0.010740	0.000415	0.282365	0.000135	749	2.6	2.4	1234	186	17
18	0.029859	0.001268	0.282429	0.000075	777	4.4	1.4	1172	107	18
19	0.020281	0.000860	0.282430	0.000119	760	4.7	2.1	1159	166	19
20	0.014124	0.000597	0.282377	0.000050	762	2.9	0.9	1224	69	20
03WN61 granite										
1	0.036029	0.001634	0.282376	0.000027	830	2.4	1.0	1259	77	1
2	0.061790	0.002744	0.282378	0.000025	829	1.8	0.9	1296	74	2
3	0.038854	0.001775	0.282461	0.000054	778	5.3	1.9	1143	155	3
4	0.114411	0.004875	0.282428	0.000047	778	2.5	1.7	1299	148	4
5	0.069044	0.003050	0.282428	0.000056	816	3.5	2.0	1232	165	5
6	0.057845	0.002625	0.282440	0.000024	769	4.1	0.9	1201	71	6
7	0.052408	0.002380	0.282471	0.000039	807	5.4	1.4	1147	113	7
8	0.046753	0.002113	0.282389	0.000024	766	2.6	0.9	1257	69	8
9	0.033836	0.001616	0.282443	0.000029	827	4.7	1.0	1164	82	9
10	0.030362	0.001410	0.282419	0.000025	784	4.0	0.9	1192	70	10
11	0.039483	0.001858	0.282489	0.000033	774	6.3	1.2	1105	94	11
12	0.047955	0.002155	0.282343	0.000034	761	0.9	1.2	1326	97	12
13	0.038741	0.001813	0.282404	0.000039	767	3.3	1.4	1225	111	13
14	0.054332	0.002594	0.282462	0.000029	634	4.9	1.1	1168	86	14
15	0.062853	0.002801	0.282474	0.000031	757	5.2	1.1	1156	93	15
16	0.072377	0.003250	0.282468	0.000030	781	4.8	1.1	1180	89	16
17	0.090824	0.004000	0.282468	0.000035	781	4.4	1.3	1205	107	17
18	0.042237	0.001899	0.282471	0.000036	748	5.6	1.3	1132	105	18
19	0.101319	0.004648	0.282467	0.000033	626	4.0	1.2	1230	101	19
20	0.058035	0.002689	0.282523	0.000054	781	7.0	1.9	1081	158	20
21	0.036253	0.001627	0.282528	0.000027	786	7.7	1.0	1043	77	21
22	0.042502	0.001945	0.282471	0.000028	782	5.6	1.0	1134	81	22
23	0.059068	0.002614	0.282511	0.000030	782	6.6	1.1	1096	89	23
24	0.053175	0.002379	0.282562	0.000056	814	8.5	2.0	1015	163	24
25	0.038142	0.001795	0.282526	0.000031	784	7.6	1.1	1049	89	25

Table 5 (*Continued*)

Spot no.	$^{176}Yb/^{177}Hf$	$^{176}Lu/^{177}Hf$	$^{176}Hf/^{177}Hf$	$\pm(2\sigma)$	U–Pb age (Ma)	$\varepsilon_{Hf}(t)$	$\pm(2\sigma)$	T_{DM} (Ma)	$\pm(2\sigma)$	Age spot
03WN65 granite										
1	0.088663	0.002880	0.282484	0.000012	777	5.5	0.4	1144	37	1.1
2	0.116841	0.003776	0.282471	0.000011	772	4.6	0.4	1193	35	10.1
3	0.071846	0.002622	0.282490	0.000011	715	5.9	0.4	1128	33	3.1
4	0.067007	0.002458	0.282523	0.000010	792	7.1	0.4	1074	29	2.1
5	0.093305	0.003624	0.282510	0.000017	680	6.1	0.6	1129	51	7.1
6	0.070214	0.002658	0.282545	0.000016	778	7.8	0.6	1048	46	6.1
7	0.080200	0.002939	0.282567	0.000023		8.4	0.8	1023	68	
8	0.054398	0.002093	0.282525	0.000031	737	7.4	1.1	1060	90	5.1
9	0.098274	0.003358	0.282527	0.000020	800	6.8	0.7	1096	60	4.1
10	0.081851	0.003089	0.282454	0.000019	762	4.4	0.7	1195	55	8.1
11	0.085220	0.002871	0.282507	0.000012	756	6.3	0.4	1110	36	9.1
12	0.054515	0.002025	0.282497	0.000022		6.4	0.8	1099	63	
13	0.077736	0.003012	0.282516	0.000016		6.6	0.6	1100	48	
14	0.112695	0.004617	0.282496	0.000014		5.0	0.5	1184	43	
15	0.073791	0.002813	0.282554	0.000014		8.1	0.5	1038	43	

Note: the spot number for the Lu–Hf isotope analysis is identified for correspondence to that for the U–Pb dating, and the U–Pb age denotes the $^{206}Pb/^{238}U$ age; the initial Hf isotope ratios were calculated either at $t = 820$ Ma or at $t = 780$ Ma following the U–Pb dating for the same sample.

4.5. Mineral O isotope

4.5.1. Volcanics

The dacites have large variations in $\delta^{18}O$ values of 4.2–10.8‰ for quartz, but small variations of 6.5–9.0‰ for zircon (Table 6 and Fig. 9). In the $\delta^{18}O$–$\delta^{18}O$ plot between zircon and other minerals (Fig. 9a–c), the data points of quartz, plagioclase and K-feldspar distribute nearly upright, suggesting O isotope disequilibrium due to high-T hydrothermal alteration.

Tuffs 03WN58 and 03WN59 have $\delta^{18}O$ values of 8.5–11.1‰ for all the measured mineral separates, showing the feature of high $\delta^{18}O$ values. Quartz–pyroxene pair from sample 03WN58 preserved high-T O isotope equilibrium (Fig. 9d). Sample 03WN59 has an unusually high $\delta^{18}O$ value of 11.1‰ for mag-

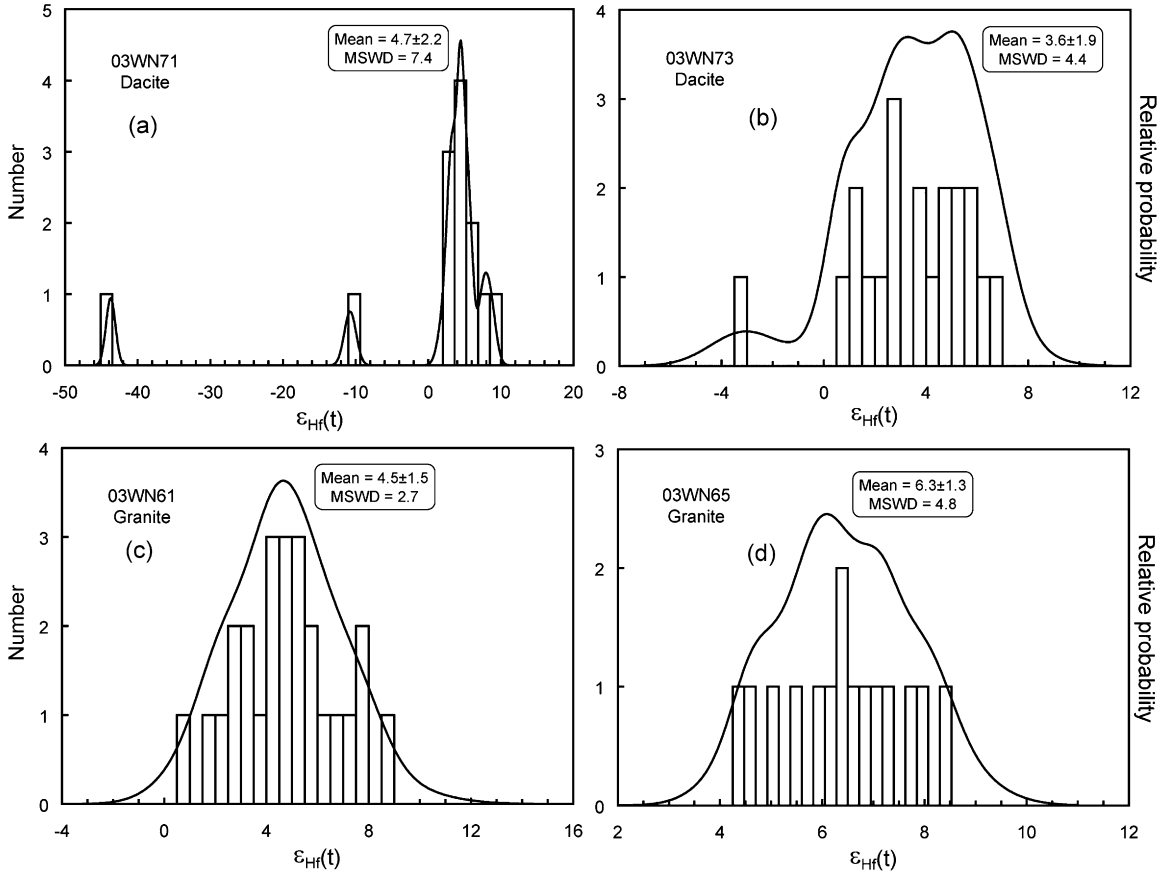

Fig. 7. Initial Hf isotope ratios for zircons from Neoproterozoic magmatic rocks in the eastern part of the Jiangnan Orogen.

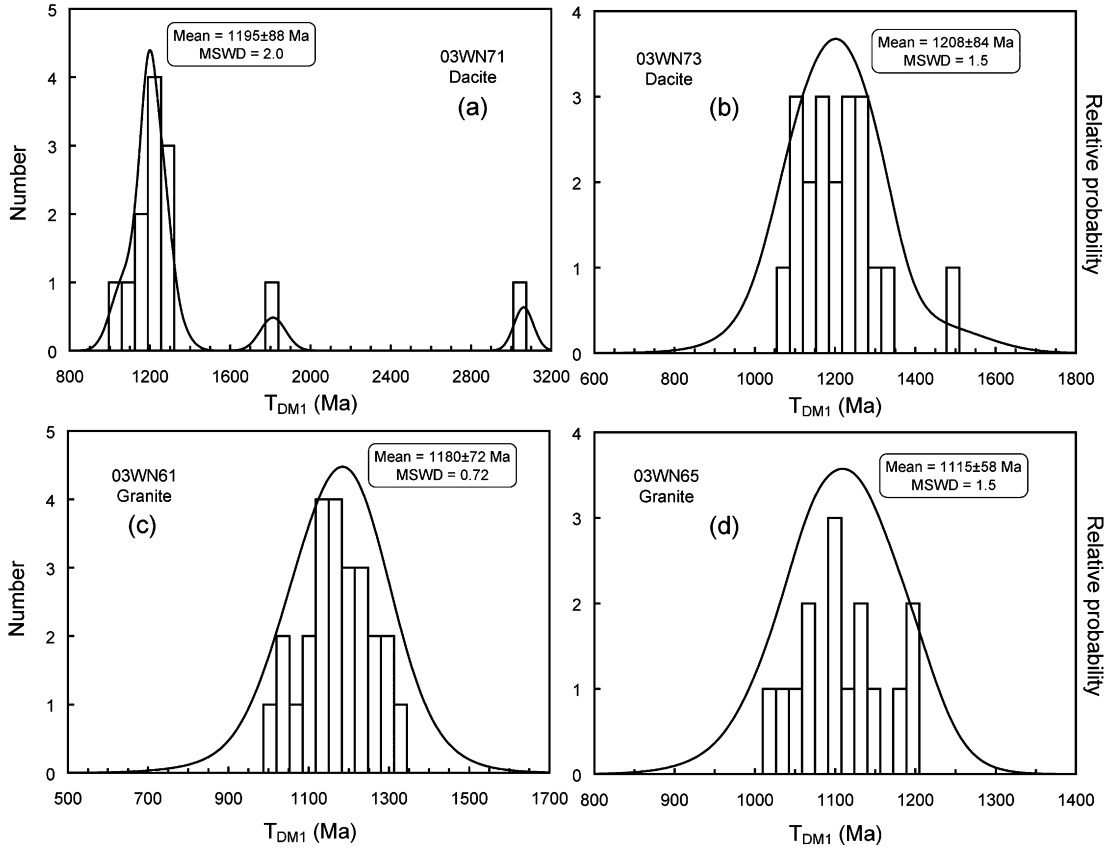

Fig. 8. Zircon Hf model ages for Neoproterozoic magmatic rocks in the eastern part of the Jiangnan Orogen.

Table 6
Oxygen isotope composition of mineral separates from magmatic rocks in the Jiangnan Orogen ($\delta^{18}O$ in permil relative to VSMOW)

Sample no.	Rock	Qz	Zr	Pl	Kfs	Px	Mt	Chl	Ep	All	Srp
Jingtan volcanics											
03WN58	Tuff	10.63				8.56					
03WN59	Tuff						11.1				9.13
03WN71	Dacite		6.52								
03WN72	Dacite	10.82	8.67	8.82	6.67						
03WN73	Dacite	9.48	8.98	6.57	5.03						
03WN74	Dacite	4.17	7.85	3.95	3.94						
Qixitian granite											
03WN60	Granite	9.27	6.32	6.44	4.93	6.43					
03WN61	Granite	7.30	6.05	4.14					1.13		
03WN62	Granite	7.45	5.78	5.16	4.78						
03WN63	Granite	7.55	6.16	4.80	4.09						
03WN64	Granite	7.38	6.33	4.84	4.31				0.85		
Lianhuashan granite											
03WN65	Granite	3.61	5.23	1.37	1.89		−4.76	−3.80			
03WN66	Granite	2.54	6.52	1.76	1.55		−6.47				
03WN67	Granite	2.26	6.27	2.38	2.51		−4.79				
03WN68	Granite	1.88	7.05	2.49	2.02						
03WN69	Granite	3.88	6.67	4.13	3.71		−4.83		−3.84		
03WN70	Granite	6.48	7.11	4.50	3.15					3.84	
05WN118	Granite	2.61	6.03	1.18	0.95		−6.95				
05WN121	Granite	1.83	5.01	1.52	1.85		−7.17				
05WN122	Granite	2.91		0.86			−5.67				
05WN123	Granite	4.15	5.45	1.91	1.83		−7.79				
05WN124	Granite	2.98		0.74	0.85						
05WN126	Granite	3.12	5.99	0.52	0.47		−10.8				

Mineral abbreviations: Qz: quartz; Zr: Zircon; Pl: plagioclase; Kfs: potassic feldspar; Px: pyroxene; Mt: magnetite; Chl: chlorite; Ep: epidote; All: allanite; Srp: serpentine.

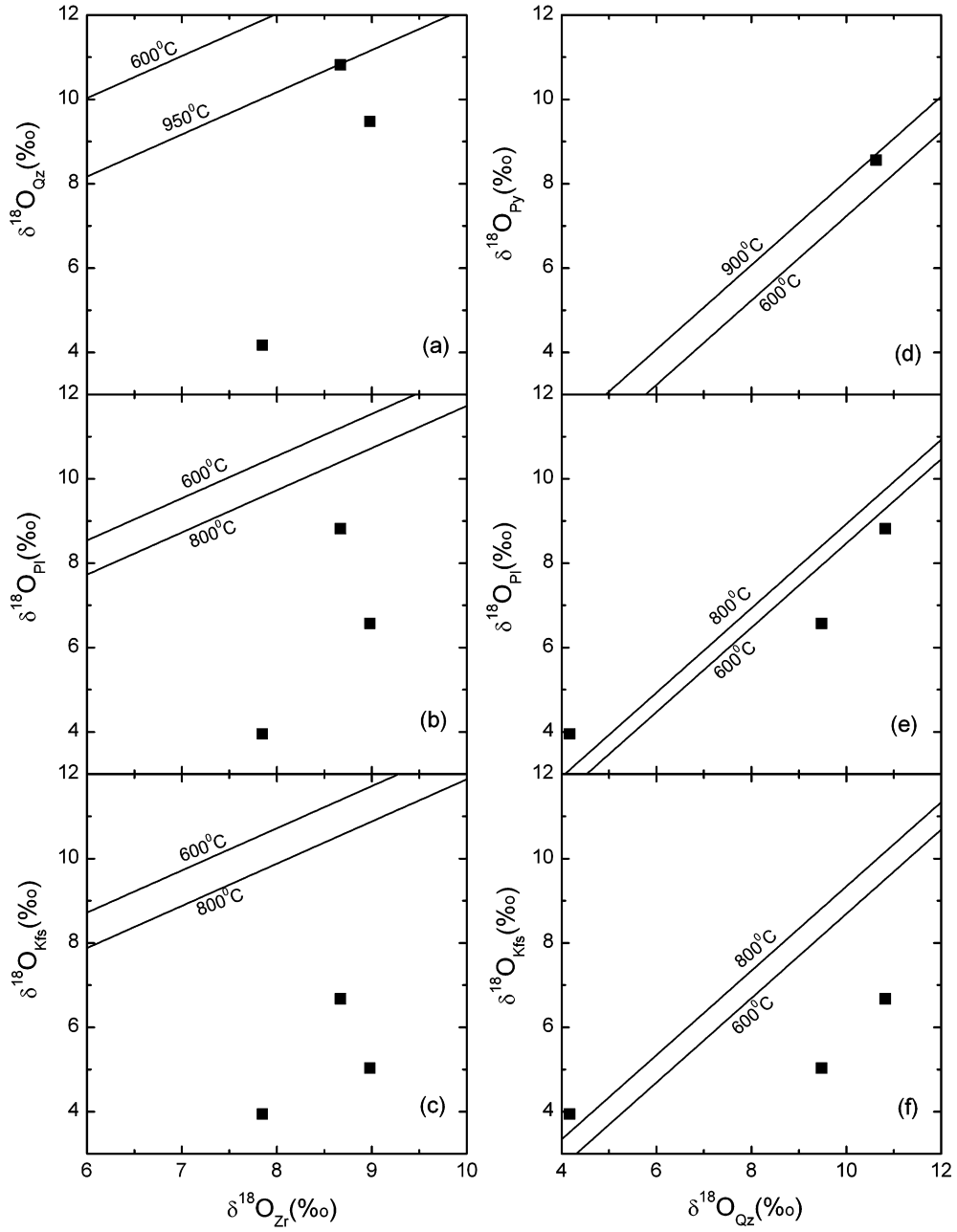

Fig. 9. Mineral $\delta^{18}O$–$\delta^{18}O$ plots for the Jingtan volcanics in the eastern part of the Jiangnan Orogen.

netite and 9.1‰ for serpentine (Table 6), significantly higher than typical mantle whole-rock $\delta^{18}O$ values of 5.7 ± 0.5‰ (Harmon and Hoefs, 1995). Because of the relatively slow rates of O diffusion (Zheng and Fu, 1998), magnetite $\delta^{18}O$ values are resistant to hydrothermal alteration at subsolidus temperatures. Thus the existence of high $\delta^{18}O$ magnetite suggests that the tuffs were influenced by post-magmatic hydrothermal alteration.

4.5.2. Granite

The granite at Shi'ershan has $\delta^{18}O$ values of 5.0–7.1‰ for zircon, 1.8–9.3‰ for quartz, 0.5–4.9‰ for K-feldspar, 0.5–6.4‰ for plagioclase, and −10.8 to −4.76‰ for magnetite (Table 6). Except for a pyroxene that has a $\delta^{18}O$ value close to equilibrium with zircon, the other minerals such as quartz, K-feldspar and plagioclase show apparent O isotope disequilibria with near-vertical slopes in the $\delta^{18}O$–$\delta^{18}O$ plot between zircon and minerals (Fig. 10). This suggests that these minerals were affected by short-term high-T hydrothermal alteration (Criss et al., 1987; Taylor, 1988). While low $\delta^{18}O$ values of 0.5–4.5‰ for feldspars can be explained by surface (oceanic or meteoric) water hydrothermal alteration at medium to high temperatures, negative $\delta^{18}O$ values as low as −10.8 to −7.2‰ clearly result from meteoric-hydrothermal alteration at high temperatures.

Oxygen isotope disequilibrium is also evident for such minerals as plagioclase, K-feldspar, epidote and magnetite (Fig. 11) that have much faster rates of O diffusion than quartz and are thus susceptible to hydrothermal alteration at medium to low temperatures (Zheng and Fu, 1998). Quartz–pyroxene and

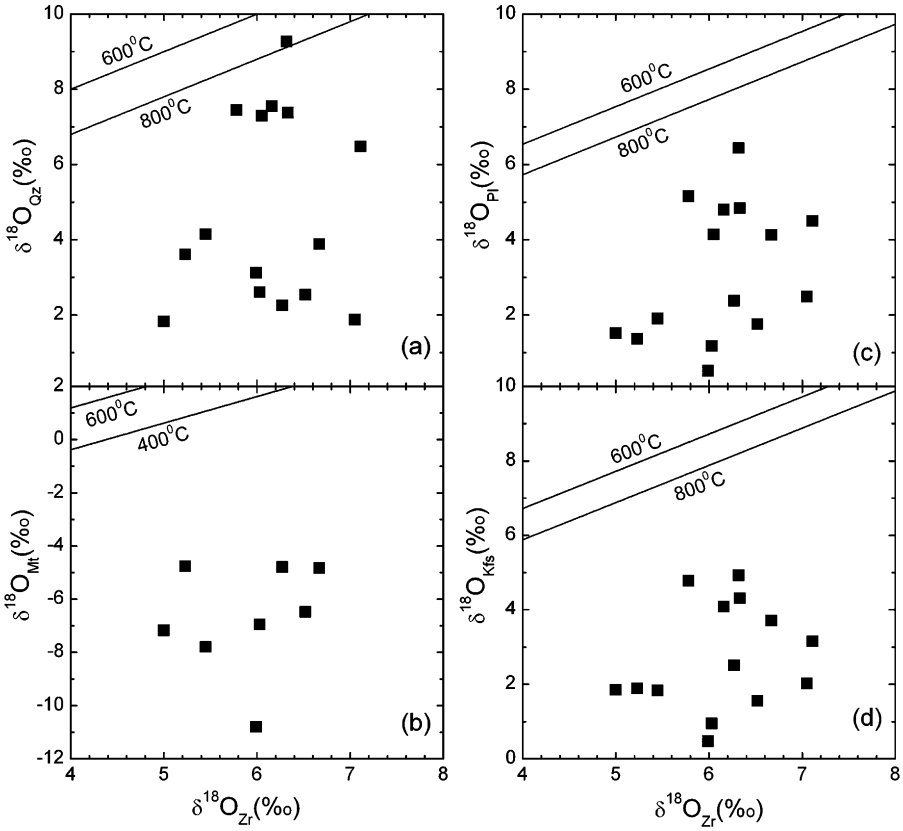

Fig. 10. $\delta^{18}O$–$\delta^{18}O$ plot between zircon and minerals from granites at Shi'ershan in the eastern part of the Jiangnan Orogen.

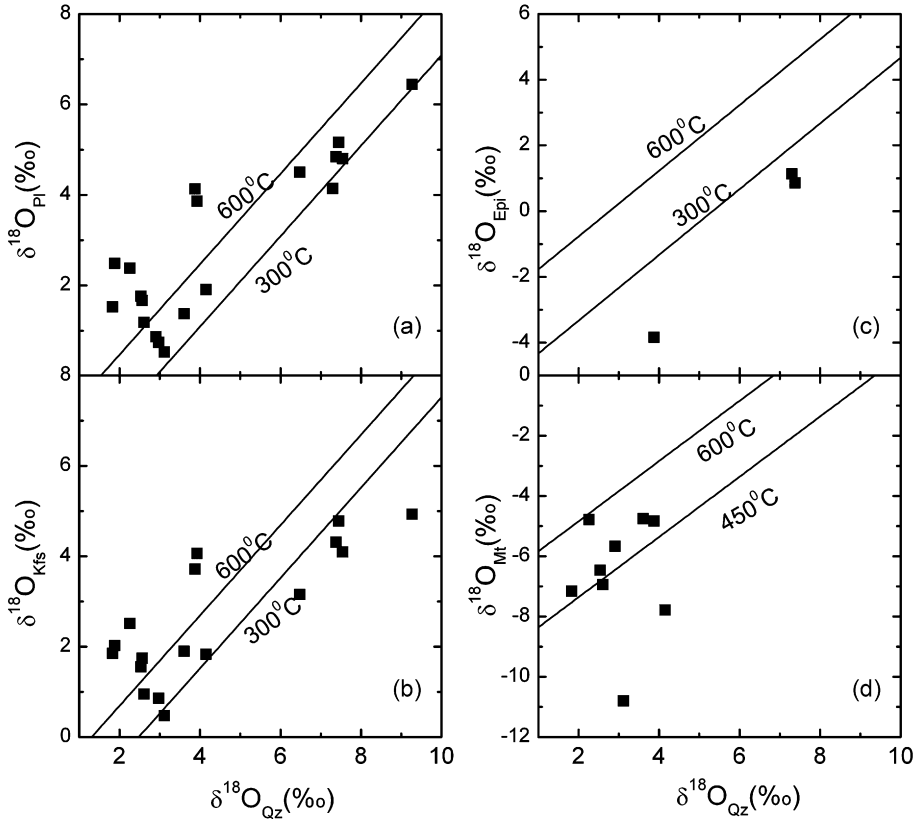

Fig. 11. $\delta^{18}O$–$\delta^{18}O$ plot between quartz and minerals from granites at Shi'ershan in the eastern part of the Jiangnan Orogen.

quartz–allanite pairs seem to show O isotope equilibria as indicated by their high O isotope temperatures of 650 and 630 °C. This suggests that the pyroxene and allanite were almost undisturbed by hydrothermal alteration at medium to low temperatures.

5. Discussion

5.1. Zircon U–Pb geochronology

For the Jingtan volcanics, CL images show that most zircons are euhedral and oscillatory zoned (Fig. 2a and b), clearly of co-magmatic origin. Some crystals exhibit structures of core-rim or core-mantle-rim (Fig. 2a), suggesting inheritance from old crustal relict. The U–Pb dating yields two consistent ages of 779 ± 7 and 773 ± 7 Ma for tuff 03WN58 and dacite 03WN73 (Fig. 3a and b). A weighted mean of 776 ± 10 Ma is calculated for them and thus is used to represent an episode of magmatism. On the other hand, an age of 820 ± 16 Ma was obtained for dacite 03WN71 (Fig. 3c), representing timing of early magmatism. The same ages of about 825 Ma are also obtained in zircon xenocrysts from samples 03WN58 and 03WN73 (Fig. 3a and b). Previous dating on the Jingtan volcanics gave a Sm–Nd isochron age of 829 ± 35 Ma (Xu et al., 1992). Therefore, the Jingtan volcanics were formed by the two episodes of volcanic eruption at ~780 and ~825 Ma, respectively.

For the three granites from Shi'ershan, CL images (Fig. 2d–f) show that they generally have similar crystal morphology and CL images except that some zircons from granite 03WN61 have rounded bright rims (Fig. 2d). The U and Th contents and Th/U ratios indicate that all of the zircons are of magmatic origin (Tables 1 and 2), and the large variations in Th and U contents may be related to hydrothermal alteration (Kempe et al., 2004; Hoskin, 2005). Furthermore, their apparent $^{206}Pb/^{238}U$ ages can be statistically subdivided into two groups (Fig. 3d–f): (1) 771 ± 7 to 777 ± 7 Ma, which are predominant in amount and represent the timing of magma crystallization; (2) 821 ± 8 to 822 ± 12 Ma, which often occur in cores and thus are interpreted as the inherited ages. Although there are some differences in zircon U–Pb ages between the different samples, they are generally consistent within the limit of errors. The young group of U–Pb ages yields a weighted mean of 775 ± 8 Ma that is interpreted to represent timing of granite crystallization. This age agrees with a SHRIMP zircon U–Pb age of 779 ± 11 Ma for the same granite (Li et al., 2003b).

The older group of U–Pb ages at about 825 Ma are consistent not only with the formation age of 820 ± 16 Ma for dacite 03WN71, but also with a SHRIMP zircon U–Pb age of 823 ± 8 Ma (Li et al., 2003a) and a LA-ICPMS zircon U–Pb age of 824 ± 6 Ma (Wu et al., 2006a) for the granodiorite in South Anhui. Thus, this group of U–Pb ages for the Shi'ershan granites are interpreted to be inherited from their source region. In this regard, the Shi'ershan granite may principally be derived from reworking of about 825 Ma igneous rocks. A single-grained TIMS zircon U–Pb age of 825 ± 3 Ma for the Shi'ershan granite was reported by Tang et al. (1997), which is its source age rather than its formation age. In either case, both old and young groups of U–Pb ages at ~825 and ~780 Ma occur in the granites and volcanics (Fig. 3). This demonstrates that the two episodes of magmatism extensively took place in the eastern part of Jiangnan Orogen.

5.2. Temperatures of magma crystallization

The Shi'ershan granite shows porphyritic to porphyroid textures, indicating its shallow emplacement. According to Zr contents and whole-rock major element composition, the zircon saturation temperatures of 760–855 °C are acquired in this study (Table 3). Because zircon is one of the earliest minerals that crystallize from magma, the Zr saturation temperatures are responsible for the temperature at which the Zr-saturated magma began crystallizing zircon (e.g., Ferreira et al., 2003). As illustrated by the CL imaging and U–Pb dating (Fig. 2d and e), there are inherited zircons occurring as cores or individual grains in the granites. This indicates that their crystallization temperature is lower than that required for complete dissolution of zircons in granitic magma. In this case, zircon saturation thermometry (T_{Zr}) yields the upper limit of temperature at which a zircon crystal could survive in a melt having the composition of the bulk rock. This provides a potential constraint on the maximum temperature of granitic magma generation (Miller et al., 2003). Thus we interpret the lowest T_{Zr} value of 760 °C as the maximum temperature of magma crystallization for the Shi'ershan granites.

According to Zr contents and whole-rock major element composition, the calculated zircon saturation temperatures (T_{Zr}) for the volcanics range from 765 to 840 °C (Table 3). In the same tectonic setting, the basalt-andesitic magma usually has higher temperatures than the granitic magma. But the calculated T_{Zr} of 765 °C for tuff 03WN58 is lower than 835–840 °C for the dacite (Table 3), indicating that the Zr saturation thermometry is not applicable to this basalt-andesitic tuff. This is consistent with the experimental protocols of Watson and Harrison (1983). Both CL imaging (Fig. 2a–c) and U–Pb dating (Fig. 3a–c) show both inherited and co-magmatic zircons from the tuff and dacite. Thus the Jingtan volcanics would also reach Zr saturation in the magma chamber, and the T_{Zr} values of 835–840 °C may give a close approximate to the temperature of magma quenching.

Since the analysed samples of dacite and granite were affected by hydrothermal alteration, O isotopes are in the state of disequilibrium between most minerals including quartz and zircon (Figs. 9–11). Nevertheless, tuff 03WN58 shows an equilibrium O isotope fractionation between quartz and pyroxene, yielding a temperature of 860 °C. This implies that the tuff did not experience significant subsolidus high-*T* hydrothermal alteration.

5.3. Mineral O isotope record of water–rock interaction

From zircon CL images and mineral O isotope compositions (Fig. 2a–c; Table 6), zircons from the volcanics were not affected by high-*T* hydrothermal alteration. Crystalline zircon is resistant to subsolidus high-*T* water–rock interaction and dry granulite-facies metamorphism and thus capable of preserving

its magmatic $\delta^{18}O$ value (Valley, 2003; Zheng et al., 2004). Therefore, the relatively high $\delta^{18}O$ values of 6.5–9.0‰ for the zircons indicate that the volcanics were derived from the high $\delta^{18}O$ source. Quartz, plagioclase and K-feldspar from the dacites have large variations of $\delta^{18}O$ values (Fig. 9), clearly due to local high-*T* hydrothermal alteration by internally derived fluid (Taylor, 1988). But the minerals from the tuffs preserve high $\delta^{18}O$ values of 8.5–11.1‰ (Table 6), and were not affected by high-*T* hydrothermal alteration. Thus, the Jingtan volcanics were partially altered by the high-*T* water–rock interaction.

All minerals from the Shi'ershan granite show large variations of $\delta^{18}O$ values (Figs. 10 and 11; Table 6), indicating the overprint of high-*T* hydrothermal alteration (Criss et al., 1987; Taylor, 1988). Obscured oscillatory zoning, resorbed rim, recrystallization, and high contents of Th and U are observed in some co-magmatic zircon (Figs. 2 and 3), consistent with the inference that the granites suffered the high-*T* hydrothermal alteration. The low $\delta^{18}O$ values of 1.8–3.9‰ for quartz are obviously caused by high-*T* hydrothermal alteration, with low $\delta^{18}O$ fluid originating from surface water (seawater or meteoric water). The lower and variable $\delta^{18}O$ values of 0.5–6.4‰ for feldspars (Table 5) require a rapid high-*T* water–rock interaction (Taylor, 1988). Quartz from the granite shows the lower and thus reversed $\delta^{18}O$ values of 1.9–9.3‰ relative to those of 5.0–7.1‰ for the coexisting zircon (Figs. 10–12). This is basically consistent with the difference in O diffusivity between zircon and quartz (Watson and Cherniak, 1997; Zheng and Fu, 1998), confirming the field-based conclusion that the quartz is easier to exchange O isotopes than zircon at high-*T* hydrothermal conditions (Wei et al., 2002).

Because of the very slow rate of O diffusion in crystalline zircon (Watson and Cherniak, 1997; Zheng and Fu, 1998), the zircon is capable of preserving its magmatic $\delta^{18}O$ value through subsequent dry granulite-facies metamorphism, subsolidus high-*T* hydrothermal alteration, and possibly magmatic assimilation or anatexis (Valley, 2003; Zheng et al., 2004). The granodiorite in South Anhui, at the western side of the Jingtan volcanics, have $\delta^{18}O$ values of 11.9–14.0‰ for quartz and 8.1–10.2‰ for zircon, showing relatively homogeneous $\delta^{18}O$ values (Fig. 12a). These indicate that their source rocks are sedimentary rocks with high $\delta^{18}O$ values. But $\delta^{18}O$ values for coexisting K-feldspar and plagioclase vary largely (Fig. 12b and c), suggesting that they suffered short-term subsolidus hydrothermal alteration during magma cooling (Wu et al., 2006a). The data points of K-feldspar and plagioclase from volcanics and granites distribute along the 45° line, apparently differ from those of granodiorite in South Anhui (Fig. 12b and c). This indicates they experienced high-*T* hydrothermal alteration (Taylor, 1988).

The zircon $\delta^{18}O$ values for the Shi'ershan granite are considerably lower than those for the Jingtan dacites and the Neoproterozoic granodiorites in South Anhui (Fig. 12a and Table 6), with variable $\delta^{18}O$ values from 5.0 to 7.1‰. They are close to $\delta^{18}O$ values of 5.3 ± 0.3‰ for normal mantle zircons (Valley et al., 1998), suggesting preservation of primary $\delta^{18}O$ values for arc-derived magma. The significant difference in zircon $\delta^{18}O$ value between different samples can be

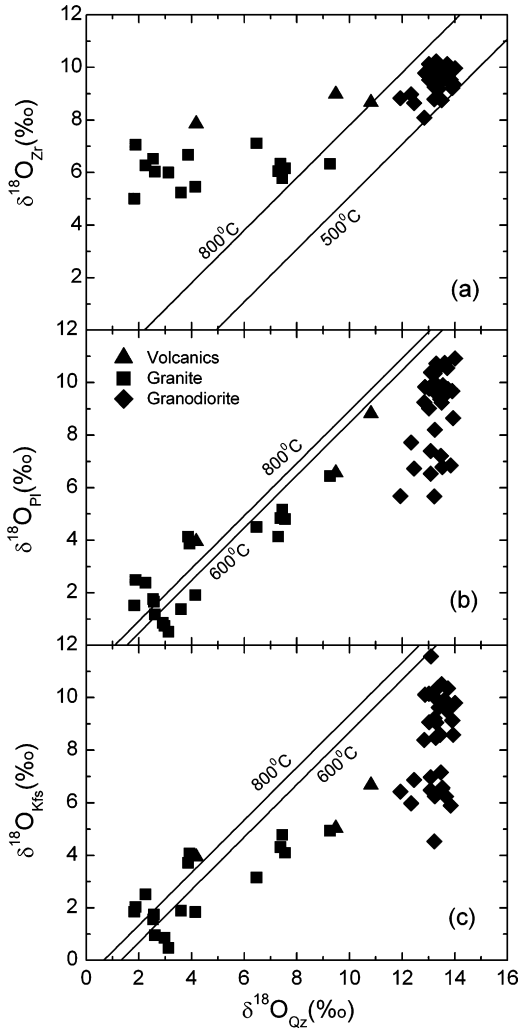

Fig. 12. $\delta^{18}O$–$\delta^{18}O$ plot between quartz and minerals from Neoproterozoic magmatic rocks in South Anhui.

explained by heterogeneous $\delta^{18}O$ distribution in the magma chamber that had not been homogenized prior to emplacement. Very short residence time is thus implied in magma chamber processes, almost contemporaneously from remelting of high-*T* hydrothermal-altered rocks to magma emplacement. Based on zircon SHRIMP U–Pb dating for S-type dacites in Neogene volcanic province of SE Spain, Zeck and Williams (2002) inferred that the time interval between anatexis to volcanic eruption is about 2–3 Ma, and measured whole-rock Rb–Sr isochron age of ca. 210 Ma was interpreted in the way that the dacites preserved the internal chemical and isotopic heterogeneity of their protoliths. Cesare et al. (2003) gave further study on zircon U–Pb ages for the Neogene S-type dacites, and found that magmatic residence time depends on the depth of partial melting. The residence time for deep-crust melts (ca. 25 km) can be up to 3 Ma, whereas that for shallow-crust melts (ca. 15 km) is less than 1 Ma. Both CAMECA zircon ^{230}Th–^{238}U ion microprobe dating (Reid et al., 1997) and ^{238}U–^{230}Th isochron dating (Heath et al., 1998) were carried out for the quaternary volcanic rocks, the obtained residence time was only 100–300 ka or even shorter. Therefore, the very short residence time is pos-

sible for the generation of variable $\delta^{18}O$ magmas in rift tectonic zones.

Except for zircon, almost all other minerals from the Shi'ershan granites have lower $\delta^{18}O$ values than normal mantle values (Table 6). This indicates that the rock-forming minerals significantly exchanged O isotopes with the low $\delta^{18}O$ surface fluid at high temperatures. The distance between the sampling locations of 05WN118 and 05WN126 is less than 2 km (Fig. 1), but their $\delta^{18}O$ values range from 1.8 to 4.2‰ for quartz (Table 6), consistent with local high-T hydrothermal alteration. If a local low $\delta^{18}O$ magma is responsible for the low $\delta^{18}O$ zircons, equilibrium $\delta^{18}O$ values are expected to occur between the coexisting minerals. This is not the case for the Shi'ershan granite. Almost all of the zircons from sample 03WN65 show dark CL and high contents of U and Th (Fig. 2e), resembling hydrothermally altered zircons in internal structure and U–Th chemistry (Kempe et al., 2004; Hoskin, 2005). Thus, channelized flow of high-T low $\delta^{18}O$ fluid occurred, with transient alteration, along microcacks during granite emplacement in association with meteoric-hydrothermal circulation. If the time of water–rock reaction would be long enough, of course, O isotope reequilibration could be achieved between the coexisting minerals.

5.4. The origin of igneous rocks

The present study shows that the volcanics and granites at Shi'ershan share many features in element and isotope geochemistry with the granodiorites in South Anhui and the metasedimentary rocks of the Shangxi Group in adjacent areas, particularly in REE and trace element partition patterns (Fig. 6) as well as Nd isotope ratios and Nd model ages (Chen and Jahn, 1998; Wu et al., 2006a). The major elements such as TiO_2 and Al_2O_3 have good correlations with SiO_2 contents (Fig. 5). This suggests a genetic connection with respect to their protolith origin of juvenile crust. Strong enrichment in LILE and LREE as well as negative anomalies in P and HFSE are a common feature of trace element partition for the continental crust that is usually assumed to originate from the chemical differentiation of arc-derived magmas (Taylor and McLennan, 1995). Thus, the arc-like patterns of trace element partition appear to be inherited from pre-existing arc-derived rocks, with variable degrees of modification by partial melting. In addition, back-arc rift basins are a potential tectonic setting that is capable of producing both MORB-like and arc-like basalts (e.g., Lawton and McMillan, 1999; Taylor and Martinez, 2003), with significant growth of juvenile crust. Arc–continent collision is a major tectonic process by which juvenile crust is accreted to continental margins to result in the continental growth (Rudnick, 1995).

Wu et al. (2006a) report that Neoproterozoic granodiorites in South Anhui were generated at 824 ± 6 Ma by remelting of water-rich sedimentary rocks that are principally derived from 882 ± 9 Ma oceanic arc precursors. The zircon $\delta^{18}O$ values for the Jingtan volcanics are basically equal to those of granodiorites in South Anhui (Table 6). Thus, the source rocks of volcanics must have experienced chemical weathering prior to deposition on the earth's surface, resulting in elevated $\delta^{18}O$ values. In contrast, the zircon $\delta^{18}O$ values for the Shi'ershan granites are relatively lower (Fig. 12a), pointing to mantle-like $\delta^{18}O$ values for their source rocks.

The inherited zircons from the Shi'ershan granite have U–Pb ages of ca. 825 Ma, implying that their source rocks are mainly from ca. 820–830 Ma source. The some volcanics in South Anhui also formed at ca. 825 Ma (Fig. 3c and d), coeval with the granodiorite (Wu et al., 2006a). Although the Shi'ershan granites share many features in element and isotope geochemistry with the volcanics and granodiorites in South Anhui, they are more evolved, with the features of more enrichment in LILE and REE, more depleted in mafic components, and stronger Eu negative anomalies than the granodiorites in South Anhui (Fig. 6c and d). Thus the Shi'ershan granites were possibly derived from the ca. 825 Ma igneous rocks that were originated from reworking of Mesoproterozoic juvenile crust. As argued by Wu et al. (2006a), it is the reworking of juvenile arc-derived crust by syn- and post-collisional magmatism that makes bulk crust composition more continental.

The presence of Mesoproterozoic juvenile crust is indicated by zircon Hf and whole-rock Nd isotopes in the Neoproterozoic magmatic rocks at the southeastern margin of the Yangtze Block (Fig. 13). While positive $\varepsilon_{Hf}(t)$ values of 3.4 ± 1.6 to 6.3 ± 1.3 are obtained from zircons in the rocks, their whole-rock analyses give neutral $\varepsilon_{Nd}(t)$ values of -2.8 to 0.7 (Wu et al., 2006a; this study). Correspondingly, zircon Hf model ages of 1.12–1.25 Ga are younger than whole-rock Nd model ages of 1.40–1.75 Ga (Fig. 13b). It appears that zircon Lu–Hf and whole-rock Sm–Nd isotope systems in arc-derived rocks were evolved in different ways, with significant difference in their element concentrations and isotope compositions. The differences between the Hf and Nd isotope results are significant, with positive deviation of the zircon $\varepsilon_{Hf}(t)$ values from the whole-rock $\varepsilon_{Nd}(t)$ values with reference to the normal terrestrial arrays of mantle and crust Hf–Nd isotope evolution (Vervoort et al., 1999). This is normally called as Hf–Nd isotope decoupling (Patchett et al., 1984). Its occurrence in S-type granitoids is basically related to preservation of initially high $\varepsilon_{Hf}(t)$ values due to zircon effect (Wu et al., 2006a; Zheng et al., 2007a). In this case, zircon Hf model ages can provide a reasonable proxy for timing of juvenile crust growth (Kemp et al., 2006; Nebel et al., 2007). Thus, the Hf model ages of 1.12 ± 0.06 to 1.25 ± 0.06 Ga for the mid-Neoproterozoic igneous rocks in South Anhui indicate the late Mesoproterozoic growth of juvenile crust by oceanic arc magmatism during the Grenvillian subduction.

On the basis of the above discussion, the origin of the mid-Neoproterozoic igneous rocks in the eastern part of the Jiangnan Orogen can be outlined as follows: (1) the Grenvillian subduction of oceanic crust between the Yangtze Block and the Cathaysia Block brought about extensive island-arc magmatism at ca. 1.3–1.1 Ga, leading to growth of juvenile crust at the southeastern margin of the Yangtze Block; (2) the arc–continent collision and syn-collisional magmatism occurred at 900 ± 20 Ma, with emplacement of arc-derived magmas and ophiolites in the suprasubduction zone; (3) due to tectonic collapse of the collision-thickened orogen during the first stage of the rifting, the S-type magmatic rocks, including 824 ± 6 Ma

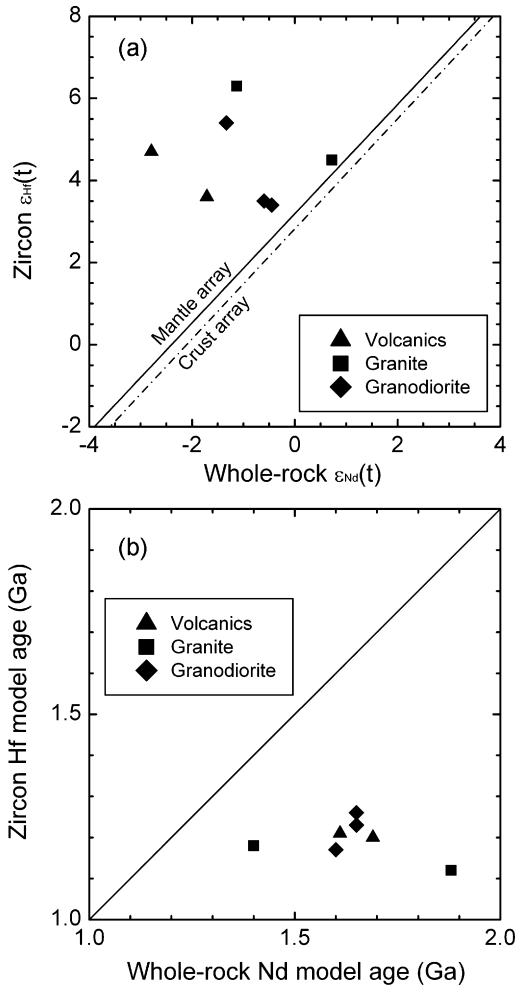

Fig. 13. Diagrams of zircon Hf and whole-rock Nd isotope relationships in Neoproterozoic magmatic rocks in the eastern part of the Jiangnan Orogen. (a) Initial Hf and Nd isotope ratios, and (b) Hf and Nd model ages.

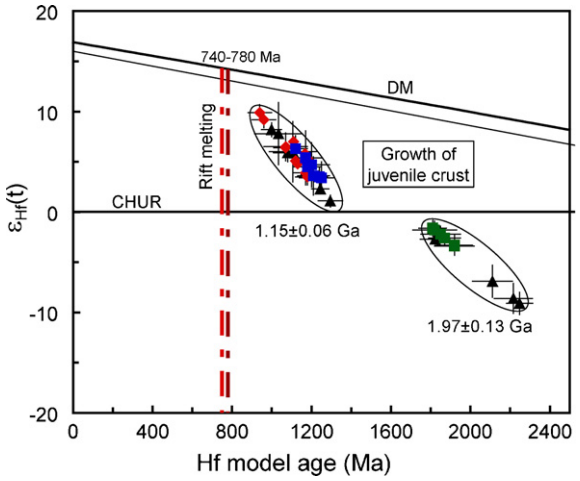

Fig. 14. The relationship between initial Hf isotope ratio and Hf model age for zircon from mid-Neoproterozoic magmatic rocks in the periphery of the Yangtze Block (data refer to Table 7). Red diamonds denotes the samples from the western margin (the Kangding Rift), block triangles denote the metaigneous rocks in the northern margin (the Dabie–Sulu Orogen), blue squares denote the samples from the southeastern margin (the eastern part of the Jiangnan Orogen), and green squares denote the samples from the southern margin (the western part of the Jiangnan Orogen). The thick line denotes the evolution of depleted mantle (DM) with a present-day $^{176}Hf/^{177}Hf = 0.28325$ and $^{176}Lu/^{177}Hf = 0.0384$ (Griffin et al., 2000), and the thin line denotes the evolution of depleted mantle that is drawn by using $\varepsilon_{Hf}(t) = 16$ at $t = 0$ Ma for MORB at present (average MORB value, Nowell et al., 1998) and $\varepsilon_{Hf}(t) = 6$ at $t = 2.7$ Ga (Corfu and Noble, 1992; Vervoort et al., 1999). (For interpretation of the references to colour in this figure legend, the reader is referred to the web version of the article.)

granodiorites and 820 ± 16 Ma volcanics, were generated by remelting of late Mesoproterozoic juvenile crust, and the granodiorites experienced short-term post-magmatic subsolidus hydrothermal alteration; (4) during the initial stage of supercontinental rifting, the 776 ± 10 Ma volcanics were generated by melting of arc-derived orogenic sediments, and the 775 ± 8 Ma granites were formed by anatexis of ca. 825 Ma igneous rocks in the rift zone. The volcanics and granites suffered high-*T* meteoric-hydrothermal alteration in response to thermal pulse of the supercontinental rifting. Collectively, the source-process relationship constrained from the mid-Neoproterozoic igneous rocks in South Anhui provides a positive test to the plate-rift model of Zheng et al. (2007a).

6. Plate-rift model for Neoproterozoic magmatism

The ages of about 830–740 Ma are a prominent period of extensive magmatism in South China. On one hand, it is interpreted as a series of magmatic products in response to the Rodinia breakup, which was hypothesized to be triggered by the mantle superplume of middle Neoproterozoic (Li et al., 2003a, 2003b, 2006). On the other hand, an island-arc origin is suggested for some of contemporaneous magmatic rocks because the trace element patterns of relevant rocks are similar to those typical evolved island-arc rocks (Zhou et al., 2002a,b, 2004, 2006a,b; Wang et al., 2004a, 2006; Zhao and Zhou, 2007). Various observations, especially zircon U–Pb ages and whole-rock trace element distributions, were employed to fit into either the plume-rift model or the slab-arc model. However, each interpretation of the observations has characteristic strengths and weaknesses. Thus, there have been hot debates involving the petrogenesis of ca. 830–740 Ma igneous rocks in South China. This is illustrated by a number of the above cited papers as well as three pairs of comment-reply between Wang et al. (2004b) and Li et al. (2004), between Zhou et al. (2007b) and Li et al. (2007a), and between Munteanu and Yao (2007) and Li et al. (2007b). Because the contemporaneous growth of juvenile crust is substantially implicated in the plume-rift and slab-arc models, the presence or absence of mid-Neoproterozoic juvenile crust can provide a geochemical test to the two models (Zheng et al., 2007a; Zhang et al., 2008).

Available Hf isotope studies of magmatic zircon indicate that two generations of juvenile crust were principally involved in the middle Neoproterozoic magmatism in the periphery of the Yangtze Block (Table 7 and Fig. 14). The old one is characterized by negative $\varepsilon_{Hf}(t)$ values of −9.1 ± 1.1 to −1.6 ± 0.8 and old Hf model ages of 1.81 ± 0.07 to 2.25 ± 0.07 Ga (a weighted mean of 1.97 ± 0.13 Ga). It occurs in the western part of the Jiangnan Orogen (Zheng et al., 2007a) and the Dabie–Sulu Orogen

Table 7
Summary of zircon U–Pb age, Lu–Hf and O isotopes for mid-Neoproterozoic magmatic rocks in the periphery of the Yangtze Block

Sample locality and rock name	Sample number	U–Pb age		Lu–Hf isotope		$\delta^{18}O$ (‰)	Reference
		t_2 (Ma)	t_1 (Ma)	$\varepsilon_{Hf}(t)$	T_{DM} (Ga)	Zircon	
Southeastern margin (the erstern part of the Jiangnan Orogen)							
Jingtan dacite	03WN71	820 ± 16		4.7 ± 2.2	1.20 ± 0.09	6.5	This study
Jingtan dacite	03WN73	773 ± 7	825 ± 11	3.6 ± 1.9	1.21 ± 0.08	9.0	This study
Shi'ershan granite	03WN61	775 ± 5	821 ± 8	4.5 ± 1.5	1.18 ± 0.07	6.1	This study
Shi'ershan granite	03WN65	771 ± 17		6.3 ± 1.3	1.12 ± 0.06	5.4	This study
Xucun granodiorite	03WN29	823 ± 7	878 ± 14	5.4 ± 2.7	1.17 ± 0.08	9.5	Wu et al. (2006a,b)
Shexian granodiorite	03WN05	823 ± 9	882 ± 8	3.4 ± 1.6	1.25 ± 0.06		Wu et al. (2006a,b)
Xiuning granodiorite	03HN49	824 ± 7	892 ± 14	3.5 ± 0.9	1.24 ± 0.04	10.1	Wu et al. (2006a,b)
Southern margin (the western part of the Jiangnan Orogen)							
Sanfang leucogranite	90113	826 ± 13*		−1.6 ± 0.8	1.81 ± 0.07	8.8	Zheng et al. (2007a)
Sanfang leucogranite	98GX9-1	826 ± 13*		−3.3 ± 1.0	1.92 ± 0.09	9.0	Zheng et al. (2007a)
Sanfang granite	97GX-1	826 ± 13*		−3.4 ± 0.8	1.92 ± 0.10	8.7	Zheng et al. (2007a)
Bendong granodiorite	98GX16	820 ± 18*		−1.8 ± 0.9	1.82 ± 0.11	9.8	Zheng et al. (2007a)
Yuanbaoshan granite	98GX6-5	824 ± 4*		−2.2 ± 0.8	1.85 ± 0.10	10.4	Zheng et al. (2007a)
Eshan granite	98KD154	819 ± 8		−2.6 ± 0.8	1.87 ± 0.08	6.8	Zheng et al. (2007a)
Western margin (Kangding Rift)							
Panzhihua granodiorite	98KD133	759 ± 11		3.9 ± 0.8	1.17 ± 0.06	6.2	Zheng et al. (2007a)
Panzhihua tonalite	98KD139	759 ± 11*		3.5 ± 0.8	1.18 ± 0.06	6.2	Zheng et al. (2007a)
Shaba gabbro	98KD104	752 ± 12		6.4 ± 1.2	1.07 ± 0.06	4.2	Zheng et al. (2007a)
Shaba gabbro	98KD111	752 ± 11		6.5 ± 1.4	1.07 ± 0.11	4.2	Zheng et al. (2007a)
Kangding tonalite	98KD36	768 ± 7		9.9 ± 0.8	0.94 ± 0.06	5.5	Zheng et al. (2007a)
Kangding granite	98KD70	751 ± 10		9.2 ± 0.8	0.96 ± 0.06	4.4	Zheng et al. (2007a)
Datian granodiorite	DT10	760 ± 14		5.1 ± 0.6	1.12 ± 0.02		Zhao et al. (2008)
Dadukou gabbro	DDK46	746 ± 10		4.8 ± 0.4	1.13 ± 0.02		Zhao et al. (2008)
Gaojiacun gabbro-diorite	PZH37	812 ± 3		7.0 ± 0.4	1.11 ± 0.01		Zhao et al. (2008)
Tongde gabbro	TD4	820 ± 13		5.3 ± 0.3	1.18 ± 0.01		Zhao et al. (2008)
Tongde gabbro	TD30	820 ± 13*		5.8 ± 0.5	1.17 ± 0.02		Zhao et al. (2008)
Northern margin (the Dabie–Sulu Orogen)							
Shuanghe metagranite	01SH13		758 ± 27	1.1 ± 0.6	1.30 ± 0.06	−4.3	Zheng et al. (2005a)
Shuanghe metagranite	01SH08		756 ± 42	3.9 ± 0.4	1.17 ± 0.04	−3.2	Zheng et al. (2005a)
Shuanghe metagranite	01SH07		758 ± 25	−2.7 ± 0.6	1.82 ± 0.07	−1.2	Zheng et al. (2006)
Shuanghe metabasite	95M22		744 ± 8	2.3 ± 0.3	1.24 ± 0.04	−4.1	Zheng et al. (2006)
Wumiao metagranite	96DB24		753 ± 47	5.9 ± 0.9	1.08 ± 0.07	−1.7	Zheng et al. (2006)
Wumiao metabasite	96DB25		749 ± 55	8.2 ± 0.7	1.00 ± 0.05	4.4	Zheng et al. (2006)
Maobei metagranite	02-I4A		785 ± 19	7.8 ± 3.1	1.03 ± 0.12	−1.9	Chen et al. (2007a)
Maobei metabasite	02-I6A		779 ± 42	6.0 ± 3.0	1.11 ± 0.12	1.1	Chen et al. (2007a)
Maobei metabasite	02-II8A			−6.9 ± 1.6	2.11 ± 0.10	−3.5	Chen et al. (2007a)
Maobei metagranite	02-II9A		783 ± 34	−9.1 ± 1.1	2.25 ± 0.07	−3.6	Chen et al. (2007a)
Maobei metabasite	02-II1(2)A			−8.6 ± 1.5	2.22 ± 0.10	−3.8	Chen et al. (2007a)

Note: * denotes the U–Pb age on the same intrusive.

of its northern margin (Zheng et al., 2005a, 2006; Chen et al., 2007a). In contrast, the young one has positive $\varepsilon_{Hf}(t)$ values of 1.1 ± 0.6 to 9.9 ± 0.8 and young Hf model ages of 0.94 ± 0.06 to 1.30 ± 0.06 Ga (a weighted mean of 1.15 ± 0.06 Ga), which occurs in the eastern part of the Jiangnan Orogen (Wu et al., 2006a; this study), the Dabie–Sulu Orogen (Zheng et al., 2006; Chen et al., 2007a) and the Kangding Rift of its western margin (Zheng et al., 2007a; Zhao et al., 2008). In particular, both old and young periods of juvenile crust growth occur in its northern margin, making this belt the most favorite place for supercontinental rifting. In either case, however, the young Hf model ages are still considerably older than the hypothesized ages of 830–740 Ma for the plume-related magmatism (Li et al., 2003a,b, 2006) or the subducted-related magmatism (Zhou et al., 2002a,b, 2004, 2006a,b; Zhao and Zhou, 2007). Even Archean lithosphere was reworked to form the mafic to felsic intrusions of about 800–830 Ma at the Yangtze Gorge in the interior of the Yangtze Block (Zhang et al., 2008). Therefore, no growth of juvenile crust is contemporaneously associated with the plume- or subducted-related magmatism during the middle Neoproterozoic in South China. This makes the two models less feasible for their petrogenesis. Instead, the plate-rift processes can well account for the Hf isotope records and other observations. Relevant arguments are further built below, with an attempt to resolve the debates between the plume-rift and slab-arc models.

If there was a mantle superplume event during the middle Neoproterozoic in South China, large igneous provinces including komatiites, flood basalts, mafic dyke swarms, and layered mafic intrusions should have formed a type of surface exposures (Ernst and Buchan, 2003). So far no such material specifically related to a mantle plume has been identified in any of the 830–740 Ma igneous rocks along the Jiangnan Orogen (Wang

et al., 2004b, 2006). No mafic large igneous provinces of any type in this age have been found in South China either (Wang et al., 2006; Zheng et al., 2007a). Thus, this period of Neoproterozoic magmatism is difficult to be interpreted as the product of mantle superplume activity. Furthermore, the plume-rift model is disfavored by the growth of juvenile crust in the late Mesoproterozoic rather than in the middle Neoproterozoic. In fact, little evidence exists so far for mantle plumes beneath the continental rifts; the presence of mantle plumes is chiefly hypothesized from large volumes of magmatic rocks associated with the rifting processes.

Although supercontinent breakup may be triggered by the impingement of a mantle superplume on the overlying lithosphere (Morgan, 1983; Richards et al., 1989; Hill, 1991; Storey and Kyle, 1997; White, 1997; Condie, 2004), it can also be caused by lithospheric extension in response to subduction (Anderson, 1982; Le Pichon and Huchon, 1984; Cox, 1988; Storey et al., 1992; Zheng et al., 2007a). The assumption that large-scale, sub-continental melting is necessarily caused by mantle plumes has also been challenged (Coltice et al., 2007), with the suggestion that continental aggregation may promote such melting without the involvement of a mantle plume. In essence, a supercontinent insulates the mantle and isolates it from subducting cooling. As a result, lateral temperature gradients and plate boundary forces occur along old plate boundaries. Because ancient collision belts are favorite places for rift magmatism and continental breakup (Dewey, 1988; Vauchez et al., 1997; Tommasi and Vauchez, 2001), attributes of orogenic lithosphere are susceptible to reactivation by extensional tectonics and thermal anomalies. Because South China was not broken up along the Jiangnan Orogen during the mid-Neoproterozoic, it appears that the tectonic transition from syn-collisional compression to post-collisional extension occurred at about 830–820 Ma; this episode of magmatism was a response to the tectonic collapse of arc–continent collision orogen (Wu et al., 2006a; Zheng et al., 2007a). Thus, the tectonic collapse of the collision-thickened orogen at the southeastern margin of the Yangtze Block gave rise to the 824 ± 6 Ma granodiorite and the 820 ± 16 Ma volcanics in South Anhui. The orogenic collapse is also accepted as a mechanism for the contemporaneous mafic to felsic magmatism at the Yangtze Gorge within the Yangtze Block (Zhang et al., 2008).

Extensive island-arc magmatism was suggested to take place at ca. 1.3–1.1 Ga in the Jiangnan Orogen between the Cathaysia and the Yangtze Blocks (e.g., Chen et al., 1991; Cheng, 1993; Shen et al., 1999). It is reinforced by the zircon Hf model ages of 1.12 ± 0.06 to 1.25 ± 0.06 Ga for the mid-Neoproterozoic magmatic rocks in the eastern part of the Jiangnan Orogen (Table 7), which record the growth of juvenile crust in this period. This points to the Grenvillian subduction of oceanic crust between the Yangtze Block and the Cathaysia Block during the late Mesoproterozoic. It was followed by formation of the Jiangnan Orogen (Charvet et al., 1996; Li et al., 2002b; Li and Li, 2003; Ye et al., 2007) due to arc–continent collision at about 900 ± 20 Ma (Wu et al., 2006a). The arc–continent syn-collisional magmatism may last till about 860 Ma as indicated by a magmatic zircon U–Pb age of 858 ± 11 Ma for ophiolitic gabbro at Huaiyu close to the Jiangshan-Shaoxing zone (Shu et al., 2006) and detrital zircon U–Pb ages of 862 ± 11 to 871 ± 6 Ma for sedimentary rocks of the Sibao/Lengjiaxi Group in the Jiangnan Orogen (Wang et al., 2007a). The zircon Hf model ages indicate that the reworked products of late Mesoproterozoic juvenile crust have geochemical similarities to the evolved arc-derived rocks. This type of igneous rocks not only underlies much of the Jiangnan Orogen, but also forms a major component in their magmatic sources.

Because of the syn- or post-collisional reworking of pre-existing arcs, the island-arc magmatism during the subduction of oceanic crust is possibly difficult to be distinguished in trace element pattern from arc-derived magmatism. Nevertheless, the Grenvillian subduction of oceanic crust is characterized by the growth of juvenile crust in the late Mesoproterozoic along the periphery of the Yangtze Block (Wu et al., 2006a; Zheng et al., 2006, 2007a; Chen et al., 2007a; Zhao et al., 2008; this study). So far no mid-Neoproterozoic ages of island-arc juvenile crust are found in South China. In other words, no mid-Neoproterozoic subduction of oceanic crust has been indicated by the contemporaneous growth of juvenile crust in South China. This can be explained by the geochemical behavior of element Zr in mantle-derived magmas. It is well established that the primary arc magmatic rocks are characterized by the depletion of HSFE (Hawkesworth et al., 1993; Tatsumi and Eggins, 1995). Thus, Zr is unsaturated in arc magmas, pointing to impossible crystallization of co-magmatic zircon from them (Zheng et al., 2006). Even if the crystallization of HSFE-poor minerals such as olivine and pyroxene could cause progressive Zr enrichment in residued melts, it remains to demonstrate if local Zr saturation is able to occur in the last batch of the residued melts after removal of the Zr-poor minerals. Nevertheless, Zr can become saturated in magmas derived from melting of arc rocks due to reworking of arc–continent collision and post-collisional collapse. As a result, zircon can only crystallize from the secondary arc-derived magmas. In this regard, it is a mistake to interpret the zircon U–Pb ages for arc-like magmatic rocks as the timing of arc magmatism. Therefore, the slab-arc model is not applicable to the mid-Neoproterozoic magmatic rocks in the periphery of the Yangtze Block. Consequently, the plate-rift model of Zheng et al. (2007a) is preferred for their petrogenesis because it is capable of not only interpreting the available observations of geology and geochemistry but also reconciling the apparently conflict arguments between the plume-rift and slab-arc models.

High Mg mafic–ultramafic rocks may provide insight into the debates between the plume-rift and slab-arc models. Such rocks were reported to occur in the southern margin of the Yangtze Block (Zhou et al., 2000; Wang et al., 2004a). Wang et al. (2007b) interpret the Neoproterozoic age of komatiitic basalts at Yiyang in the middle part of the Jiangnan Orogen as "the first solid petrological evidence" for the proposed ca. 825 Ma mantle plume in South China. The high-Mg basalts are assumed as if they were generated by melting of an anomalously hot mantle source with potential temperatures of >1500 °C at anhydrous conditions. However, it fails to consider an alternative mechanism of melting at hydrous conditions to produce komatiites (Allegre, 1982; Parman et al., 1997; Stone et al., 1997) and the effect of hydrothermal alteration on the target rocks. Ultrahigh-pressure

experiments also show that komatiitic melts can be produced by partial melting of hydrous mantle even at normal temperature (Kawamoto and Holloway, 1997; Asahara et al., 1998; Asahara and Ohtani, 2001). As argued by Grove and Parman (2004), komatiites can be produced by hydrous melting at shallow mantle depths in oceanic subduction environments. Furthermore, the Rodinia breakup by the plume impingement is inconsistent with the fact that South China was not broken up along the Jiangnan Orogen where the high-Mg basalts were emplaced during the mid-Neoproterozoic. In contrast, contemporaneous andesitic to basaltic lavas are known to occur in the same region (Wang et al., 2004a), with significant alteration resulting in a possible increase of MgO concentrations and difficult recognition of phenocryst minerals in the komatiitic texture. This favors the possibility that they are all the product of subduction-zone magmatism. Thus, it is possible that the Yiyang komatiitic basalts were generated in the Grenville-type subduction zone during the convergence between the Cathaysia and Yangtze Blocks. In other words, they may be generated by partial melting of subarc refractory mantle after extraction of typical arc melts. Moreover, zircons are recovered from the Yiyang komatiitic basalts (Wang et al., 2007b), in sharp conflict with the element geochemistry of mantle plume and island arc basalts because Zr is unsaturated in them (Zheng et al., 2006). Depletion of HSFE in mafic–ultramafic cumulates from the first generation of plume and arc melts is also inconsistent with zircon growth from them. In this regard, two groups of zircon U–Pb ages at 862 ± 6 and 823 ± 6 Ma (Wang et al., 2007b) can be reinterpreted as two events reworking the primary high-Mg basalts, respectively, in response to the arc–continent collision and the tectonic collapse along the Jiangnan Orogen. Therefore, no mantle plume has been definitely demonstrated to occur at Yiyang in the middle Neoproterozoic.

Continental convergence involves the progressive impingement of buoyant or highstanding terranes with subduction zones. All scales and variations exist on this theme between the collision of seamounts and seamount chains with arc through the collision of oceanic plateaux and microcontinents with arc to the collision of large continental masses. The scale of collision dictates the style, duration and intensity of the resulting strain systems and sequences (Dewey et al., 1986). Converging continental margins are generally irregular and strain sequences are usually diachronous along great strike lengths along suture zones. Prior to terminal continental collision, one or both continental margins may have had a long and complex history of exotic terrane assembly. Thus, convergent plate boundaries between continent–arc–continent collision belts such as the Jiangnan Orogen in South China, is wide, diffuse and complicated zones where relative plate displacements are converted into complex strains and smaller block-bounding displacements, with variable degrees of low- to middle-grade metamorphism and syn-collision magmatism. This contrasts with continent–continent collision belts such the Dabie–Sulu orogenic belt, which are generally narrow, relatively high-pressure metamorphic zones without syn-collision arc magmatism (Ernst and Liou, 1995; Zheng et al., 2005b).

Available data of geochronology and geochemistry indicate that the late Mesoproterozoic magmatism is dominated by submarine volcanic eruptions due to the Grenvillian subduction of oceanic lithosphere and subsequent convergence toward the supercontinent Rodinia. This brought about large amounts of arc complexes along convergent plate margins, with some occurrences of back-arc rift basalts. The arc complexes contain only minor reworked pyroclastic deposits derived from contemporaneous subaerial eruptions, and subaerial andesite volcanoes on thickened continental crust seem to be almost absent in this period. The late Mesoproterozoic arc magmatic rocks occur not only in the southeastern margin of the Yangtze Block (i.e. the Jiangnan Orogen; Wang et al., 2004a,b, 2006; Wu et al., 2006a; Zheng et al., 2007a), but also in its northern margin including the Dabie–Sulu Orogen (Chen et al., 2007a; Zhao et al., 2007) and the Qinling Orogen (Gao et al., 1996; Ling et al., 2003). It is possible that the Yangtze Block would serve as a proto-continent during the Rodinia assembly, which was collided with oceanic and continental arcs along its periphery to result in continental accretion and supercontinental assembly during the early Neoproterozoic. Nevertheless, most of these arc rocks were reworked by arc–continent collision magmatism at 960–860 Ma and post-collisional magmatism at 830–740 Ma. This is particularly prominent for those occurring in the periphery of the Yangtze Block, mainly involving zircon U–Pb dates of 960–800 Ma (e.g., Zhou et al., 2002a; Chen et al., 2006; Xiao et al., 2007; Ye et al., 2007). Therefore, reworking of the arc rocks may be the basic reason for zircon growth from them and the possible misidentification of arc magmatic events from zircon U–Pb dates.

The mid-Neoproterozoic S-type granites extensively occur along the Jiangnan Orogen (Li et al., 2003b; Wu et al., 2006a). The zircon Hf model ages for these granites suggest that their sources are geochemically characterized by the arc-derived rocks of late Mesoproterozoic ages in the eastern part but middle Paleoproterozoic ages in the western part (Wu et al., 2006a; Zheng et al., 2007a; this study). Thus, the Jiangnan Orogen appears to have been a collision orogen between continent, arc and continent subsequent to the Grenvillian subduction of oceanic crust during the late Mesoproterozoic. The Hf model ages of 1.12 ± 0.06 to 1.25 ± 0.06 Ga for the arc-type juvenile crust (Table 7) are significantly older than the assumed age of about 750 Ma for the Rodinia breakup (Zheng et al., 2006). The final amalgamation of the Yangtze and Cathaysia Block is indicated by the intensive arc–continent collision magmatism at 880–860 Ma. Thus, this episode of collision possibly marks the final assembly of Rodinia in South China. Nevertheless, transformation of tectonic regime from compression to extension in the periphery of the Yangtze Block may take place as early as 850–840 Ma. This is indicated by a SHRIMP zircon U–Pb age of 849 ± 7 Ma for dolerite at Shenwu in the eastern part of the Jiangnan Orogen (Li et al., 2008) and a LA-ICP-MS zircon U–Pb age of 844 ± 2 Ma for syenite at Fangcheng in the Qinling Orogen (Bao et al., 2008). Zircons from the Shenwu dolerite also contain two groups of inherited U–Pb ages at ~900 and ~940 Ma (Li et al., 2008), respectively, recording two episodes of magmatism by the arc–continent collision.

Convergent continental margins generally involve continental accretion by a series of arc-continent collision. Orogenic

belts of such collision are characterized by the formation of mountain belts that are significantly affected by deformation, metamorphism and magmatism. The evolution of continental margins, in the frame of plate tectonic theory, is summarized by the Wilson cycle which holds that opening and closing of oceans are spatially related and give rise to the tectonic patterns observed on the Earth. Nevertheless, continental and oceanic plates may move coherently on the Earth because the parts experience similar forces or constraints. As a result, localized extension occurs at plate boundaries in response to horizontal compression, and continental rifting develops in response to oceanic subduction. Furthermore, the orogenic cycle comprises a period of arc–continent or continent−continent collision accommodated by crustal thickening. Partial melting due to the arc-continent collision leads to the first time of the chemical differentiation of juvenile mafic crust towards less mafic composition. Gravity is usually considered as the main driving force causing extension and thinning of previously thickened crust (e.g., Dewey, 1988; Molnar and Lyon-Caen, 1988). Gravity-driven flow leading to net thinning of the orogenic crust is defined as gravitational collapse (Rey et al., 2001). Three mechanisms have been proposed to trigger the gravitational collapse of an orogenic belt and explain the transition from crustal thickening to crustal thinning (Molnar et al., 1993): (1) a sudden increase of gravitational potential energy related to asthenospheric upwelling, which can be caused either by convective removal or by delamination of the lithospheric mantle root; (2) a decrease in the strength at the base of the zone of thickened crust due to thermal weakening; (3) a decrease in the tectonic force applied at the boundary of the system related to a decrease in plate convergence. In either case, partial melting due to the orogenic collapse results in the second time of the chemical differentiation of continental crust towards the felsic composition.

On the other hand, mid-Neoproterozoic magmatism is dominated by the subaerial emplacement of both intrusive and eruptive rocks due to the supercontinental rifting. The rift-related complexes contain reworked igneous and sedimentary rocks derived from both juvenile and ancient crusts, with a progressive increase in rock proportion from subaerial to submarine eruptions in response to the Rodinia breakup. Turbulent tectonic environments were probably the norm in the mid-Neoproterozoic, specifically with growth and reworking of juvenile crust along the rift tectonic zones that were developed along pre-existing arc–continent collision orogens. Because the arc–continent collisional orogens would take several 100 million years to achieve thermo-mechanical stability, they would be tectonically weak and thus susceptible to be rifted away (Murphy et al., 2006; Thomas, 2006). This may have occurred along the northern margin of South China during its separation from Rodinia (Zheng et al., 2006; Chen et al., 2007a). The lithospheric extension would drive the supercontinnetal breakup, with the fragments moving away from the thermal and gravitational anormalies. Newly formed plate boundaries are association with transient bursts of magmatism, including large igneous provinces from previously insulated regions of the mantle. As a consequence, the tectonic evolution from supercontinental assembly to breakup involves a global reorganization of plates, stress, and motions.

Syn-rift magmatism also occurred intensively at about 780–740 Ma in South China (Li et al., 2003a; Zheng et al., 2004; Zhao and Zhou, 2007; Zhou et al., 2007a; Tang et al., 2008; Wang et al., 2008), which may be related to the tectonic transition from supercontinental rift to breakup. Zircon Hf isotope studies indicate that this period of magmatism is associated with reworking of not only late Mesoproterozoic juvenile crust but also middle Paleoproterozoic juvenile crust (Zheng et al., 2006, 2007a; Chen et al., 2007a; Zhao et al., 2008; this study). It appears that the crustal reworking during the supercontinental rifting also causes the chemical differentiatio of continental crust towards the felsic composition. As implicated in the plate-rift model of Zheng et al. (2007a), far-field plate boundary forces are considered as the primary driving force of lithospheric extsension and rift magmatism during the mid-Neoproterozoic, with consequent rifting of South China from Rodinia. Many intracontinental rifts initiate or localize at formerly convergent boundaries in response to ridge subduction, in back-arc settings, or along suture zones following arc–continent or continent–continent collision. Substantial along-strike variations in the composition and source of rifting magmas, with these variations controlled by pre-rift tectonics and magmatism of the formerly convergent margin, may thus be common along many of rifted continental margins. Different from the slab-arc model and the plume-rift model, therefore, the plate-rift model does not appeal the occurrence of either a mantle superplume or arc magmatism in the period of 830–740 Ma. Instead, it assumes arc-continnet collision at 960–860 Ma along the periphery of the Yangtze Block following the Grenvillian subduction of oceanic crust, and interprets the 830–800 Ma magmatism as the tectonic collapse of arc–continent collision orogens and the 780–740 Ma magmatism as a result of supercontinental rifting.

As implicated in the plate-rift model, the rifting has a profound influence on the continental evolution of South China, fundamentally controlling lithospheric thinning and supercontinental breakup at mid-Neoproterozoic. The extensional thinning of crust and mantle lithosphere produces local upwelling of warm asthenosphere to replace thinned lithosphere. Additional heat is released by adiabatic decompression, producing partial melting and rift-associated magmatism. The emplacement of advected warmer material causes lateral temperature gradients, which can induce small-scale convection to create significant additional horizontal stresses that further advance rifting, magmatism and other lithosphere-scale processes. As a response to the supercontinental breakup in the interior of South China, the tectonic collapse of the early Neoproterozoic arc–continent collision orogens took place in the Jiangnan Orogen. This also results in the development of middle and late Neoproterozoic rift basins between the Yangtze and Cathaysia Blocks.

In view of the above arguments, the plate-rift model for petrogenesis of Neoproterozoic igneous rocks in South China is outlined as follows (Fig. 15). (a) The subduction of oceanic crust occurred in the periphery of the Yangtze Block, leading to extensive island-arc magmatism with growth of juvenile crust at about 1.3–1.1 Ga (Fig. 15a). (b) Following the closure of back-arc

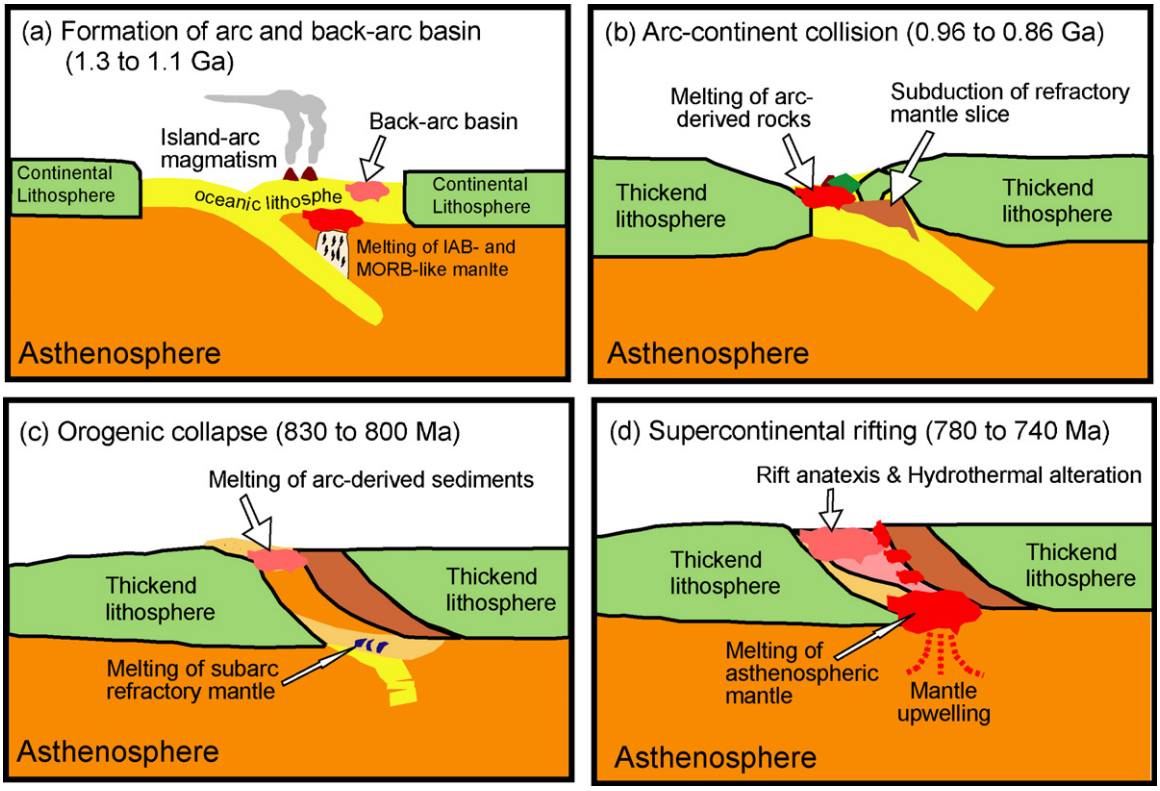

Fig. 15. The plate-rift model for petrogenesis of Neoproterozoic magmatic rocks in South China (abstracted from Wu et al., 2006a; Zheng et al., 2006, 2007a; Chen et al., 2007a). Unlike the slab-arc model, it assumes arc magmatism at about 1.3–1.1 Ga rather than 860–740 Ma in the periphery of the Yangtze Block. In addition, two processes of arc–continent collision and post-collisional collapse are emphasized to take place at 960–860 and 830–820 Ma, respectively, resulting in reworking of preexisting arc rocks in arc–continent orogens. Thus, it interprets the 830–800 magmatism as being due to the orogenic collapse rather than a mantle superplume as hypothesized by the plume-rift model. Therefore, lithospheric extension is assumed to trigger supercontinental breakup and associated syn-rift magmatism at 780–740 Ma, with high-T meteoric water–rock interaction in rift tectonic zones and local remelting of hydrothermally altered low $\delta^{18}O$ rocks.

basins, arc–continent collision and syn-collisional magmatism occurred at about 960–860 Ma to result in remelting of arc rocks during the Rodinia assembly (Fig. 15b). These two processes have been often overlooked in studying the magmatic rocks of collisional orogens, but particularly emphasized in the plate-rift model. (c) Tectonic collapse of the collision-thickened orogen occurred at about 830–800 Ma (Fig. 15c), causing different types of magmatism by reworking of either late Mesoproterozoic or middle Paleoproterozoic juvenile crust. Melting of subarc refractory mantle could be brought about by thermal pulse of this episode, producing high-Mg basalts. (d) Syn-rift magmatism developed intensively in response to the tectonic evolution from supercontinental rift to breakup (Fig. 15d), with local generation of juvenile crust by melting of asthenospheric mantle in volcanic rifted margin, accompanying high-T meteoric water–rock interaction and local melting of collapsed calderas. Nevertheless, supercontinental breakup can be caused by either lithospheric extension or impingement of a mantle superplume. Although growth of juvenile crust in this period could be associated with plume-related magmatism, the lithopsheric extension mechanism is preferred before the mantle superplume is geologically identified in South China. It is also questionable to interpret high-Mg mafic to ultramafic rocks as a product by partial melting of the mantle plume because recent petrographic and experimental observations support their petrogenesis by melting of subarc or subcontinental mantle lithospheres under hydrous conditions.

The plate-rift model assumes a tectonic rock cycle surrounding the Yangtze Block during the Rodinia assembly and breakup from the Mesoproterozoic to Neoproterozoic. It includes the subduction of oceanic crust, island-arc magmatism, the closure of backarc basins, arc–continent collision and juvenile crust melting, chemical erosion and sedimentary burial, post-collisional collapse and rift anatexis, and finally supercontinental rifting. While the first half of the cycle proceeds from the subduction of oceanic crust at 1.3–1.1 Ga to the tectonic collapse of arc–continent collision orogens at about 830–800 Ma, the second half keeps pace with the tectonic evolution from supercontinental rift to breakup at about 780–740 Ma. This cycle not only mixed the newly derived mantle material with sedimentary component, but also effectively differentiated the chemical composition of juvenile mafic crust. In this regard, the chemical differentiation of continental crust is closely associated with the plate-rift processes in the history of the Earth. This may provide an additional way to resolve the compositional paradox of continental crust that has changed from basaltic to andesitic one. If partial melting occurs in the garnet stability field to form TTG and/or adakatic rocks, the density of residual phase can become greater and greater due to progressive extraction of felsic melts. As a consequence, the accumulation of high-density garnet in

the mafic residue can eventually lead to its gravitational sinking into the mantle, leaving less mafic rocks in the continental crust. Intensive meteoric water–rock interactions mostly occurred in the northern margin of the Yangtze Block at ~780 and ~750 Ma, respectively, resulting in locally low $\delta^{18}O$ magmas due to caldera collapse in the volcanic rifted margin (Zheng et al., 2004, 2006, 2007b; Wu et al., 2007). As a response to the Rodinia breakup in South China, the tectonic collapse of the Neoproterozoic arc-continent collisional orogens occurred in preexisting and new continental margins to result in the development of rift basins and anorogenic magmatism. Such portion of plate-rift processes may occur episodically in intracontinental orogens since the Late Archean, providing a causal link between plate tectonics and continental dynamics.

7. Conclusions

Two episodes of middle Neoproterozoic magmatism intensively occur in the eastern part of the Jiangnan Orogen that formed by arc–continent collision during the early Neoproterozoic. They are pre-rift one at about 825 Ma and syn-rift one at about 780 Ma, respectively. Both episodes of magmatism were originated from reworking of juvenile arc-derived crust that primarily formed during the late Mesoproterozoic in response to the Grenvillian subduction of oceanic crust between the Yangtze Block and the Cathaysia Block. The pre-rift granodiorites and volcanics were derived from remelting of orogenic sediments, with local high-*T* hydrothermal alteration by internally derived fluid. The syn-rift granites and volcanics formed by anatexis of the pre-rift igneous rocks in the orogenic root, with extensive high-*T* hydrothermal alteration by fluid of meteoric origin. Although the Jiangnan Orogen did not breakup during rifting of South China from the supercontinent Rodinia, the two episodes of magmatism are a response to lithospheric extension during the tectonic evolution from supercontinental rift to breakup.

The growth of juvenile crust occurred as island-arc magmatism at 1.3–1.1 Ga in the periphery of the Yangtze Block. Then the juvenile crust was reworked by the several episodes of magmatism, respectively, due to arc–continent collision at 960–860 Ma, post-collisional collapse at 830–800 Ma, and rift anatexis at 780–740 Ma. Because the growth of juvenile crust occurred in the late Mesoproterozoic rather than the middle Neoproterozoic, neither the plume-rift model nor the slab-arc model is applicable to origin of the 830–740 Ma magmatic rocks in South China. Therefore, the plate-rift model is preferred for their petrogenesis, with lithospheric extsension as the driving force of supercontinental rifting. It is capable of not only interpreting available geological and geochemical observations, but also reconciling apparently conflict arguments between the plume-rift and slab-arc models. In particular, the two processes of arc–continent collision and syn-collisional magmatism are emphasized to occur at 960–860 Ma in the periphery of the Yangtze Block. They have to be taken into account when deciphering the origin of magmatic rocks in continent–arc–continent collision orogens. The final assembly of the Yangtze Block with the Cathaysia Block is marked by the intensive arc–continent collision magmatism at 880–860 Ma, which may also be a terminal episode of amalgamating Rodinia in South China. The rift magmatism at 780–740 Ma leads to the chemical reworking of both late Mesoproterozopic and middle Paleoproterozoic juvenile crusts. Multi-stages of partial melting in the plate-rift processes are also considered as the cause for the compositional evolution of juvenile crust from basaltic to andesitic to granitic one. This may provide an alternative way to resolve the compositional paradox of continental crust.

Acknowledgments

This study was supported by funds from the Chinese Academy of Sciences (KZCX3-SW-141) and the Natural Science Foundation of China (40334036). We appreciate the assistance of S.Q. Yang with SHRIMP dating, Z.Y. Chen with zircon CL imaging, D.E. Wang with field work, B. Gong, X.P. Zha and Y.B. Zhao with O isotope analyses. We thank Dr. Y.J. Wang and one anonymous reviewer for their comments that help improvement of the presentation.

References

Allegre, C.J., 1982. Genesis of Archaic komatiites in a wet ultramafic subducted plate. In: Arndt, N.T., Nisbet, E.G. (Eds.), Komatiites. George Allen Unwin, Winchester, MA, pp. 495–500.

Andersen, T., 2002. Correction of common lead in U–Pb analyses that do not report ^{204}Pb. Chem. Geol. 192, 59–79.

Anderson, D., 1982. Hotspots, polar wander, Mesozoic convection and the geoid. Nature 297, 391–393.

Asahara, Y., Ohtani, E., Suzuki, A., 1998. Melting relations of hydrous and dry mantle compositions and the genesis of komatiites. Geophys. Res. Lett. 25, 2201–2204.

Asahara, Y., Ohtani, E., 2001. Melting relations of the hydrous primitive mantle in the CMAS–H_2O system at high pressures and temperatures, and implications for generation of komatiites. Phys. Earth Planet. Interior 125, 31–44.

Bao, Z.W., Wang, Q., Bai, G.D., Zhao, Z.H., Song Y.W., Liu, X.M., 2008. Geochronology and geochemistry of the Fangcheng Neoproterozoic alkali-syenites in East Qinling orogen and its geodynamic implications. Chin. Sci. Bull. 53, doi:10.1007/s11434-008-0113-z.

Bindeman, I.N., Valley, J.W., 2001. Low $\delta^{18}O$ rhyolites from yellowstone: magmatic evolution based on analysis of zircon and individual phenocrysts. J. Petrol. 42, 1491–1517.

Blichert-Toft, J., Albarede, F., 1997. The Lu–Hf geochemistry of chondrites and the evolution of the mantle-crust system. Earth Planet. Sci. Lett. 148, 243–258.

Cesare, B., Gómez-Pugnaire, M.T., Rubatto, D., 2003. Residence time of S-type anatectic magmas beneath the Neogene Volcanic Province of SE Spain: a zircon and monazite SHRIMP study. Contrib. Miner. Petrol. 146, 28–43.

Charvet, J., Shu, L.S., Shi, Y.S., Guo, L.Z., Faure, M., 1996. The building of south China: collision of Yangzi and Cathaysia blocks, problems and tentative answers. J. Southeast Asian Earth Sci. 13, 223–235.

Chen, J.F., Jahn, B.M., 1998. Crustal evolution of southeastern China: evidence from Sr, Nd and P b isotope compositions of granitoids and sedimentary rocks. Tectonophysics 284, 101–133.

Chen, J.F., Foland, K.A., Xing, F.M., Xu, X., Zhou, T.X., 1991. Magmatism along the southeast margin of the Yangtze and Cathysia block of China. Geology 19, 815–818.

Chen, Z.H., Lu, S.N., Li, H.K., Li, H.M., Xiang, Z.Q., Zhou, H.Y., Song, B., 2006. Constrainting the role of the Qinling orogen in the assembly and breakup of Rodinia: Tectonic implications for Neoproterozoic granite occurrences. J. Asian Earth Sci. 28, 99–115.

Chen, R.-X., Zheng, Y.-F., Zhao, Z.-F., Tang, J., Wu, F.-Y., Liu, X.-M., 2007a. Zircon U–Pb ages and Hf isotopes in ultrahigh-pressure metamorphic rocks

from the Chinese Continental Scientific Drilling project. J. Metamorph. Geol. 25, 873–894.

Chen, J.F., Zheng, Y.-F., Zhao, Z.-F., Li, B., Xie, Z., Gong, B., Qian, H., 2007b. Relationships between O isotope equilibrium, mineral alteration and Rb–Sr chronometric validity in granitoids: implications for determination of cooling rate. Contrib. Miner. Petrol. 153, 251–271.

Cheng, H., 1993. Geochemistry of Proterozoic island-arc volcanic rocks in northwest Zhejiang. Geochemica 1, 18–27 (in Chinese with English abstract).

Chu, N.C., Taylor, R.N., Chavagnac, V., Nesbitt, R.W., Boella, R.M., Milton, J.A., Germain, C.R., Bayon, G., Burton, K., 2002. Hf isotope ratio analysis using multi-collector inductively coupled plasma mass spectrometry: an evaluation of isobaric interference corrections. J. Anal. At. Spectrom. 17, 1567–1574.

Coltice, N., Phillips, B.R., Bertrand, H., Ricard, Y., Rey, P., 2007. Global warming of the mantle at the origin of flood basalts over supercontinents. Geology 35, 391–394.

Condie, K.C., 2004. Supercontinents and superplume events: distinguishing signals in the geologic record. Phys. Earth Planet Inter. 146, 319–332.

Corfu, F., Noble, S.R., 1992. Genesis of the southern Abitibi Greenstone belt, Superior Province, Canada: Evidence from zircon Hf isotope analysis using a single filament technique. Geochim. Cosmochim. Acta 56, 2081–2097.

Corfu, F., Hanchar, J.M., Hoskin, P.W.O., Kinny, P., 2003. Altas of zircon textures. Rev. Miner. Geochem. 53, 469–500.

Cox, K.G., 1988. The Karoo province. In: Macdougall, J.D. (Ed.), Continental Flood Basalts. Kluwer Academic, Dordrecht, pp. 239–271.

Criss, R.E., Gregory, R.T., Taylor Jr., H.P., 1987. Kinetic theory of oxygen isotope exchange between minerals and water. Geochim. Cosmochim. Acta 51, 952–960.

DePaolo, D.J., 1988. Neodymium Isotope Geochemistry: An Introduction. Springer-Verlag, New York, 181 pp.

Dewey, J.F., 1988. Extensional collapse of orogens. Tectonics 7, 1123–1139.

Dewey, J.F., Hempton, M.R., Kidd, W.S.F., Saroglu, F., Şengör, A.M.C., 1986. Shortening of continental lithosphere: the neotectonics of Eastern Anatolia—a young collision zone. Geol. Soc. Spec. Publ. 19, 3–36.

Ernst, R.E., Buchan, K.L., 2003. Recognizing mantle plume in the geological record. Ann. Rev. Earth Planet Sci. 31, 469–523.

Ernst, W.G., Liou, J.G., 1995. Contrasting plate-tectonic styles of the Qinling–Dabie–Sulu and Franciscan metamorphic belts. Geology 23, 253–256.

Ferreira, V.P., Valley, J.W., Sial, A.N., Spicuzza, M.J., 2003. Oxygen isotope compositions and magmatic epidote from two contrasting metaluminous granitoids, NE Brazil. Contrib. Miner. Petrol. 145, 205–216.

Gao, S., Zhang, B.-R., Li, Z.-J., Wang, D.-P., Ouyang, J.-P., Xie, Q.-L., 1996. Geochemical evidence for Proterozoic tectonic evolution of the Qinling Orogenic Belt and its adjacent margins of North China and Yangtze Cratons. Precambr. Res. 80, 23–48.

Giletti, B.J., 1986. Diffusion effects on oxygen isotope temperatures of slowly cooled igneous and metamorphic rocks. Earth Planet. Sci. Lett. 77,218–228.

Griffin, W.L., Pearson, N.J., Elusive, E., Jackson, S.E., van Achtenberg, E., O'Reilly, S.Y., She, S.R., 2000. The Hf isotope composition of carbonic mantle: LAM-MC-ICPMS analysis of zircon megacrysts in kimberlites. Geochim. Cosmochim. Acta 64, 133–147.

Grove, T.L., Parman, S.W., 2004. Thermal evolution of the Earth as recorded by komatiites. Earth Planet. Sci. Lett. 219, 173–187.

Harmon, R.S., Hoefs, J., 1995. Oxygen isotope heterogeneity of the mantle deduced from global ^{18}O systematics of basalts from different geotectonic setting. Contrib. Miner. Petrol. 120, 95–114.

Hawkesworth, C.J., Gallagher, K., Hergt, J.M., McDermott, F., 1993. Mantle and slab contributions in arc magmas. Ann. Rev. Earth Planet Sci. 21,175–204.

Heath, E., Turner, S.P., Macdonald, R., Hawkesworth, C.J., van Calsteren, P., 1998. Long magma residence times at an island arc volcano (Soufriere, St. Vincent) in the Lesser Antilles: evidence from ^{238}U–^{230}Th isochron dating. Earth Planet. Sci. Lett. 160, 49–63.

Hill, R.I., 1991. Starting plumes and continental break-up. Earth Planet. Sci. Lett. 104, 398–416.

Hoskin, P.W.O., 2005. Trace-element composition of hydrothermal zircon and the alteration of Hadean zircon from the Jack Hills, Australia. Geochim. Cosmochim. Acta 69, 637–648.

Iizuka, T., Hirata, T., 2005. Improvements of precision and accuracy in in situ Hf isotope microanalysis of zircon using the laser ablation-MC-ICPMS technique. Chem. Geol. 220, 121–137.

Jahn, B.-m., Condie, K.C., 1995. Evolution of the Kaapvaal Craton as viewed from geochemical and Sm–Nd isotopic analyses of intracratonic pelites. Geochim. Cosmochim. Acta 59, 2239–2258.

Kawamoto, T., Holloway, J.R., 1997. Melting temperature and partial melt chemistry of H_2O-saturated mantle peridotite to 11 gigapascals. Science 276, 240–243.

Kelemen, P.B., Hanghoj, K., Greene, A.R., 2004. One view of the Geochemistry of subduction-related magmatic arcs, with an emphasis on primitive andesite and lower crust. Treatise Geochem. 3, 593–660.

Kemp, A.I.S., Hawkesworth, C.J., Paterson, B.A., Kinny, P.D., 2006. Episodic growth of the Gondwana supercontinent from hafnium and oxygen isotopes in zircon. Nature 439, 580–583.

Kempe, U., Bombach, K., Matukov, D., Schlothauer, T., Hutschenreuter, J., Wolf, D., Sergeev, S., 2004. Pb/Pb and U/Pb zircon dating of subvolcanic rhyolite as a time marker for Hercynian granite magmatism and Sn mineralization in the Eibenstock granite, Erzgebirge, Germany: considering effects of zircon alteration. Miner. Deposita 39, 646–669.

Lawton, T.F., McMillan, N.J., 1999. Arc abandonment as a cause for passive continental rifting: comparison of the Jurassic Mexican Borderland rift and the Cenozoic Rio Grande rift. Geology 27, 779–782.

Le Pichon, X., Huchon, P., 1984. Geoid, Pangea and convection. Earth Planet. Sci. Lett. 67, 123–135.

Li, W.X., Li, X.H., 2003. Adakitic granites within the NE Jiangxi ophiolites, South China: geochemical and Nd isotopic evidence. Precambr. Res. 122, 29–44.

Li, Z.X., Zhang, L.H., Powell, C.M., 1995. South China in Rodinia: part of the missing link between Australia-East Antarctica and Laurentia? Geology 23, 407–410.

Li, Z.X., Li, X.H., Kinny, P.D., Wang, J., 1999. The breakup of Rodinia: did it start with a mantle plume beneath South China? Earth Planet. Sci. Lett. 173, 171–181.

Li, X.H., Liu, Y., Tu, X.L., Hu, G.Q., Zeng, W., 2002a. Precise determination of chemical compositions in rock samples using ICP-AES and ICP-MS: a comparative study of sample digestion techniques of alkali fusion and acid dissolution. Geochimica 31, 289–294 (in Chinese with English abstract).

Li, Z.-X., Li, X.H., Zhou, H., Kinny, P.D., 2002b. Grenville-aged continental collision in South China: new SHRIMP U–Pb zircon results and implications for Rodinia configuration. Geology 30, 163–166.

Li, Z.X., Li, X.H., Kinny, P.D., Wang, J., Zhang, S., Zhou, H., 2003a. Geochronology of Neoproterozoic syn-rift magmatism in the Yangtze Craton, South China and correlations with other continents: evidence for a mantle superplume that broke up Rodinia. Precambr. Res. 122, 85–109.

Li, X.H., Li, Z.X., Ge, W.C., Li, W.X., Liu, Y., Wingate, M.T.D., 2003b. Neoproterozoic granitoids in South China: crustal melting above a mantle plume at ca. 825 Ma? Precambr. Res. 122, 45–83.

Li, X.-H., Li, Z.-X., Ge, W.C., Zhou, H.W., Li, W.X., Liu, Y., Wingate, M.T.D., 2004. Reply to the comment: Mantle plume-, but not arc-related Neoproterozoic magmatism in South China. Precambr. Res. 132, 405–407.

Li, W.-X., Li, X.-H., Li, Z.-X., 2005. Neoproterozoic bimodal magmatism in the Cathaysia Block of South China and its tectonic significance. Precambr. Res. 136, 51–66.

Li, X.-H., Li, Z.-X., Sinclair, J.A., Li, W.-X., Carter, G., 2006. Revisiting the "Yanbian Terrane": implications for Neoproterozoic tectonic evolution of the western Yangtze Block, South China. Precambr. Res. 151, 14–30.

Li, X.-H., Li, Z.-X., Sinclair, J.A., Li, W.-X., Carter, G., 2007a. Reply to the comment by Zhou et al. on: "Revisiting the "Yanbian Terrane": implications for Neoproterozoic tectonic evolution of the western Yangtze Block, South China" [Precambr. Res. 151 (2006) 14–30] [Precambr. Res. 154 (2007) 153–157]. Precambr. Res. 155, 318–323.

Li, X.-H., Li, Z.-X., Sinclair, J.A., Li, W.-X., Carter, G., 2007b. Understanding dual geochemical characters in a geological context for the Gaojiacun intrusion: Response to Munteanu and Yao's discussion [Precambrian Res. 154 (2007) 164–167]. Precambr. Res. 155, 328–332.

Li, X.-H., Li, W.-X., Li, Z.-X., Liu, Y., 2008. 850-790 Ma bimodal volcanic and intrusive rocks in northern Zhejiang, South China: A major episode

of continental rift magmatism during the breakup of Rodinia. Lithos 102, 341–357.
Ling, W.-L., Gao, S., Zhang, B.-R., Li, H.-M., Liu, Y., Cheng, J.-P., 2003. Neoproterozoic tectonic evolution of the northwestern Yangtze craton, South China: implications for amalgamation and break-up of the Rodinia Supercontinent. Precambr. Res. 122, 111–140.
Liu, B.G., 1997. Analysis on the evolutionary features and origin of Shi'ershan superunit granite in Western Zhejiang. Geol. Zhejiang 13, 39–46 (in Chinese with English abstract).
Ludwig, K.R., 2001. Users Manual for Isoplot/Ex (rev. 2.49): A Geochronological Toolkit for Microsoft Excel. Berkeley Geochronology Center, Special Publication, No.1a, 55 pp.
Machado, N., Simonetti, A., 2001. U–Pb dating and Hf isotopic composition of zircons by laser ablation-MC-ICP-MS. In: Sylvester, P. (Ed.), Laser-Ablation-ICPMS in the Earth Sciences: Principles and Applications, 29. Short Course of Mineral Assoc. Canada, pp. 121–146.
McDonough, W.F., Sun, S.S., 1995. The composition of the earth. Chem. Geol. 120, 223–253.
Middlemost, E.A.K., 1994. Naming materials in the magma/igneous rock system. Earth Sci. Rev. 37, 215–224.
Miller, C.F., McDowell, S.M., Mapes, R.W., 2003. Hot and cold granite? Implications of zircon saturation temperatures and preservation of inheritance. Geology 31, 529–532.
Molnar, P., Lyon-Caen, H., 1988. Some physical aspects of the support, structure, and evolution of mountain belts. Geol. Soc. Am. Spec. Paper v. 218, 179–207.
Molnar, P., England, P., Martinod, J., 1993. Mantle dynamics, uplift of the Tibetan plateau, and the Indian monsoon. Rev. Geophys. 31, 357–396.
Morgan, W.J., 1983. Hotspot tracks and the early rifting of the Atlantic. Tectonophysics 94, 123–139.
Munteanu, M., Yao, Y., 2007. The Gaojiacun intrusion: Rift- or subduction-related?: comment on "Revisiting the "Yanbian Terrane": Implications for Neoproterozoic tectonic evolution of the western Yangtze Block, South China" by Li et al. (2006) [Precambr. Res. 151 (2006) 14–30]. Precambr. Res. 155, 324–327.
Murphy, J.B., Gutierrez-Alonso, G., Nance, R.D., Fernandez-Suarez, J., Keppie, J.D., Quesada, C., Strachan, R.A., Dostal, J., 2006. Origin of the Rheic Ocean: rifting along a Neoproterozoic suture? Geology 34, 325–328.
Nebel, O., Nebel-Jacobsen, Y., Mezger, K., Berndt, J., 2007. Initial Hf isotope compositions in magmatic zircon from early Proterozoic rocks from the Gawler Craton, Australia: a test for zircon model ages. Chem. Geol. 241, 23–37.
Nowell, G.M., Kempton, P.D., Noble, S.R., Fitton, J.G., Saunders, A.D., Mahoney, J.J., Taylor, R.N., 1998. High precision Hf isotope measurements of MORB and OIB by thermal ionisation mass spectrometry: Insights into the depleted mantle. Chem. Geol. 149, 211–233.
Parman, S.W., Dann, J.C., Grove, T.L., de Wit, M.J., 1997. Emplacement conditions of komatiite magmas from the 3.49 Ga Komati formation, Barberton Greenstone Belt, South Africa. Earth Planet. Sci. Lett. 150, 303–323.
Patchett, P.J., White, W.M., Feldmann, H., Kielinczuk, S., Hofmann, A.W., 1984. Hafnium/rare earth element fractionation in the sedimentary system and crustal recycling into the Earth's mantle. Earth Planet. Sci. Lett. 69, 365–378.
Reid, M.R., Coath, C.D., Harrison, T.M., McKeegan, K.D., 1997. Prolonged residence times for the youngest rhyolites associated with Long Valley Caldera: ^{230}Th–^{238}U ion microprobe dating of young zircons. Earth Planet. Sci. Lett. 150, 27–39.
Rey, P., Vanderhaeghe, O., Teyssier, C., 2001. Gravitational collapse of the continental crust: definitions, regimes, mechanisms and modes. Tectonophysics 342, 435–449.
Richards, M.A., Duncan, A.R., Courtillot, V.E., 1989. Flood basalts and hot-spot tracks plume heads and tails. Science 246, 103–107.
Rudnick, R.L., 1995. Making continental crust. Nature 378, 571–578.
Scherer, E., Munker, C., Mezger, K., 2001. Calibration of the lutetium–hafnium clock. Science 293, 683–687.
Shen, W.Z., Ling, H.F., Li, W.X., Huang, X.L., Wang, D.Z., 1999. Study on the Nd–Sr isotopic compositions of granitoids in SE China. Geol. J. China Univ. 5 (1), 22–32 (in Chinese with English abstract).
Shu, L.S., Faure, M., Jiang, S.Y., Yang, Q., Wang, Y.J., 2006. SHRIMP zircon U–Pb age, litho- and biostratigraphic analyses of the Huaiyu Paleozoic-early Mesozoic collision. Episodes 29, 244–252.
Stacey, J.S., Kramers, J.D., 1975. Approximation of terrestrial lead isotope evolution by a two-stage model. Earth Planet. Sci. Lett. 26, 207–221.
Stone, W.E., Deloule, E., Larson, M.S., Lesher, C.M., 1997. Evidence for hydrous high-MgO melts in the Precambrian. Geology 25, 143–146.
Storey, B.C., Kyle, P.R., 1997. An active mantle mechanism for Gondwana breakup. South Africa J. Geol. 100, 283–290.
Storey, B.C., Alabaster, T., Hole, M.J., Pankhurst, R.J., Wever, H.E., 1992. Role of subduction–plate boundary forces during the initial stages of Gondwana break-up: evidence from the proto-Pacific margin of Antarctica. In: Storey, B.C., Alabaster, T., Pankhurst, R.J. (Eds.), Magmatism and the Causes of Continental Break-up, 68. Spec. Publ. Geol. Soc. Lond., pp. 149–164.
Sun, S.S., McDonough, W.F., 1989. Chemical and isotopic systematics of oceanic basalt: implications for mantle composition and processes. In: Sanders, A.D., Norry, M.J. (Eds.), Magmatism in the Ocean Basins. Geol. Soc. Spec. Publ., 42, pp. 313–345.
Tang, H.F., Zhang, G.H., Zhou, X.M., Liu, B.G., 1997. A post-orogenic granite batholith: the age and genesis of Shi'ershan granite. J. Nanjing Univ. (Nat. Sci.) 33 (4), 587–595 (in Chinese with English abstract).
Tang, J., Zheng, Y.-F., Wu, Y.-B., Gong, B., Zha, X.P., Liu, X.M., 2008. Zircon U–Pb age and geochemical constraints on the tectonic affinity of the Jiaodong terrane in the Sulu orogen, China. Precambr. Res. 161, 389–418.
Tatsumi, Y., Eggins, S., 1995. Subduction Zone Magmatism. Blackwell Science, Oxford, 211 pp.
Taylor Jr., H.P., 1977. Water/rock interactions and the origin of H_2O in granitic batholiths. J. Geol. Soc. Lond. 133, 509–558.
Taylor Jr., H.P., 1988. Oxygen, hydrogen, and strontium isotope constraints on the origin of granites. Trans. R. Soc. Edinburgh 79, 317–338.
Taylor, B., Martinez, F., 2003. Back-arc basin basalt systematics. Earth Planet. Sci. Lett. 210, 481–497.
Taylor, S.R., McLennan, S.M., 1995. The geochemical evolution of the continental crust. Rev. Geophys. 33, 241–265.
Thomas, W.A., 2006. Tectonic inheritance at a continental margin. GSA Today 16 (2), doi:10.1130/1052-5173.2006.016.
Tommasi, A., Vauchez, A., 2001. Continental rifting parallel to ancient collisional belts: an effect of the mechanical anisotropy of the lithospheric mantle. Earth Planet. Sci. Lett. 185, 199–210.
Valley, J.W., 2003. Oxygen isotopes in zircon. Rev. Miner. Geochem. 53, 343–385.
Valley, J.W., Kitchen, N., Kohn, M.J., Niendorf, C.R., Spicuzza, M.J., 1995. UWG-2, a garnet standard for oxygen isotope ratio: strategies for high precision and accuracy with laser heating. Geochim. Cosmochim. Acta 59, 5223–5231.
Valley, J.W., Kinny, P.D., Schulze, D.J., Spicuzza, M.J., 1998. Zircon metacryst from kimberlite: oxygen isotope variability among mantle melts. Contrib. Miner. Petrol. 133, 1–11.
Vauchez, A., Barruol, G., Tommasi, A., 1997. Why do continents break-up parallel to ancient orogenic belts? Terra Nova 9, 62–66.
Vervoort, J.D., Patchett, P.J., Blichert-Toft, J., Albarede, F., 1999. Relationships between Lu–Hf and Sm–Nd isotopic systems in the global sedimentary system. Earth Planet. Sci. Lett. 168, 79–99.
Wang, J., Li, Z.X., 2003. History of Neoproterozoic rift basins in South China: implications for Rodinia break-up. Precambr. Res. 122, 141–158.
Wang, X.L., Zhou, J.C., Qiu, J.S., Gao, J.F., 2004a. Geochemistry of the Meso- to Neoproterozoic basic-acid rocks from Hunan Province, South China: implications for the evolution of the western Jiangnan orogen. Precambr. Res. 135, 79–103.
Wang, X.L., Zhou, J.C., Qiu, H.S., Gao, H.F., 2004b. Comment on "Neoproterozoic granitoids in South China: crustal melting above a mantle plume at ca. 825 Ma?" by X.-H. Li et al. Precambr. Res. 132, 401–403.
Wang, X.-L., Zhou, J.-C., Qiu, J.-S., Zhang, W.-L., Liu, X.-M., Zhang, G.-L., 2006. LA-ICP-MS zircon geochronology of the Neoproterozoic igneous rocks from Northern Guangxi, South China: Implications for tectonic evolution. Precambr. Res. 145, 111–130.
Wang, X.-L., Zhou, J.-C., Griffin, W.L., Wang, R.-C., Qiu, J.-S., O'Reilly, S.Y., Xu, X.S., Liu, X.-M., Zhang, G.-L., 2007a. Detrital zircon geochronol-

ogy of Precambrian basement sequences in the Jiangnan orogen: dating the assembly of the Yangtze and Cathaysia Blocks. Precambr. Res. 159, 117–131.

Wang, X.-C., Li, X.-H., Li, W.-X., Li, Z.-X., 2007b. Ca. 825 Ma komatiitic basalts in South China: first evidence for >1500 °C mantle melts by a Rodinia mantle plume. Geology 35, 1103–1106.

Wang, X.-L., Zhou, J.-C., Qiu, J.-S., Jiang, S.-Y., Shi, Y.-R., 2008. Geochronology and geochemistry of Neoproterozoic mafic rocks from western Hunan, South China: implications for petrogenesis and post-orogenic extension. Geol. Mag. 145, 215–233.

Watson, E.B., Cherniak, D.J., 1997. Oxygen diffusion in zircon. Earth Planet. Sci. Lett. 148, 527–544.

Watson, E.B., Harrison, T.M., 1983. Zircon saturation revisited: temperature and composition effects in a variety of crustal magma types. Earth Planet. Sci. Lett. 64, 295–304.

Wei, C.-S., Zheng, Y.-F., Zhao, Z.-F., Valley, J.W., 2002. Oxygen and neodymium isotope evidence for recycling of juvenile crust in northeast China. Geology 30, 375–378.

White, R.S., 1997. Mantle plume origin for the Karoo and Ventersdorp flood basalts, South Africa. S. Afr. J. Geol. 100, 271–282.

Wiedenbeck, M., Alle, P., Corfu, F., Griffin, W.L., Meier, M., Oberli, F., von Quadt, A., Roddick, J.C., Spiegel, W., 1995. Three natural zircon standards for U–Th–Pb, Lu–Hf, trace element and REE analyses. Geostand. Newsl. 19, 1–23.

Williams, I.S., 1998. U–Th–Pb geochronology by ion microprobe. In: McKibben, M.A., Shanks, III W.C., Ridley, W.I. (Eds.), Applications of Microanalytical Techniques to Understanding Mineralizing Processes. Rev. Econ. Geol. vol. 7, pp. 1–35.

Woodhead, J., Hergt, J., Shelley, M., Eggins, S., Kemp, R., 2004. Zircon Hf-isotope analysis with an excimer laser, depth profiling, ablation of complex geometries, and concomitant age estimation. Chem. Geol. 209, 121–135.

Wu, R.X., Zheng, Y.F., Wu, Y.B., Zhao, Z.F., Zhang, S.B., Liu, X.M., Wu, F.Y., 2006a. Reworking of juvenile crust: element and isotope evidence from Neoproterozoic granodiorite in South China. Precambr. Res. 146, 179–212.

Wu, F.-Y., Yang, Y.-H., Xie, L.-W., Yang, J.-H., Xu, P., 2006b. Hf isotopic compositions of the standard zircons and baddeleyites used in U–Pb geochronology. Chem. Geol. 234, 105–126.

Wu, Y.-B., Zheng, Y.-F., Tang, J., Gong, B., Zhao, Z.-F., Liu, X.M., 2007. Zircon U–Pb dating of water–rock interaction during Neoproterozoic rift magmatism in South China. Chem. Geol. 246, 65–86.

Xiao, L., Zhang, H.-F., Ni, P.-Z., Xiang, H., Liu, X.-M., 2007. LA-ICP-MS U–Pb zircon geochronology of early Neoproterozoic mafic-ultramafic intrusions from NW margin of the Yangtze Block, South China: Implication for tectonic evolution. Precambr. Res. 154, 221–235.

Xu, B., Guo, L.Z., Shi, Y.S., 1992. Proterozoic Plutons and Several Episodes of Collision Orogen in Neighbor Area of Anhui, Zhejiang, and Jiangxi. Publishing House of Geology, Beijing (in Chinese).

Xu, P., Wu, F., Xie, L., Yang, Y., 2004. Hf isotopic compositions of the standard zircons for U–Pb dating. Chin. Sci. Bull. 49, 1642–1648.

Ye, M.-F., Li, X.-H., Li, W.-X., Liu, Y., Li, Z.-X., 2007. SHRIMP zircon U–Pb geochronological and whole-rock geochemical evidence for an early Neoproterozoic Sibaoan magmatic arc along the southeastern margin of the Yangtze Block. Gondwana Res. 12, 144–156.

Yuan, H.-L., Gao, S., Liu, X.-M., Li, H.-M., Gunther, D., Wu, F.-Y., 2004. Accurate U–Pb age and trace element determinations of zircon by laser ablation-inductively coupled plasma mass spectrometry. Geostand. Newsl. 28, 353–370.

Zeck, H.P., Williams, I.S., 2002. Inherited and magmatic zircon from Neogene Hoyazo cordierite dacite, SE Spain—anatectic source rock provenance and magmatic evolution. J. Petrol. 43, 1089–1104.

Zhang, S.-B., Zheng, Y.-F., Wu, Y.-B., Zhao, Z.-F., Gao, S., Wu, F.-Y., 2006. Zircon isotope evidence for ≥3.5 Ga continental crust in the Yangtze craton of China. Precambr. Res. 146, 16–34.

Zhang, S.-B., Zheng, Y.-F., Zhao, Z.-F., Wu, Y.-B., Liu, X.M., Wu, F.-Y., 2008. Neoproterozoic anatexis of Archean lithosphere: Geochemical evidence from felsic to mafic intrusives at Xiaofeng in the Yangtze George, South China. Precambr. Res. 163, 210–238.

Zhao, J.-H., Zhou, M.-F., 2007. Geochemistry of Neoproterozoic mafic intrusions in the Panzhihua district (Sichuan Province, SW China): implications for subduction-related metasomatism in the upper mantle. Precambr. Res. 152, 27–47.

Zhao, Z.-F., Zheng, Y.-F., Wei, C.-S., Gong, B., 2004. Temporal relationship between granite cooling and hydrothermal uranium mineralization at Dalongshan in China: a combined radiometric and oxygen isotopic study. Ore Geol. Rev. 25, 221–236.

Zhao, Z.-F., Zheng, Y.-F., Chen, R.-X., Xia, Q.-X., Wu, Y.-B., 2007. Element mobility in mafic and felsic ultrahigh-pressure metamorphic rocks during continental collision. Geochim. Cosmochim. Acta 71, 5244–5266.

Zhao, J.-H., Zhou, M.-F., Yan, D.-P., Yang, Y.-H., Sun, M., 2008. Zircon Lu–Hf isotopic constraints on Neoproterozoic subduction-related crustal growth along the western margin of the Yangtze Block, South China. Precambr. Res. 163, 189–209.

Zheng, Y.F., 1989. Influence of the nature of the initial Rb–Sr system on isochron validity. Chem. Geol. 80, 1–16.

Zheng, Y.F., 1991. Calculation of oxygen isotope fractionation in metal oxides. Geochim. Cosmochim. Acta 55, 2299–2307.

Zheng, Y.F., 1993a. Calculation of oxygen isotope fractionation in anhydrous silicate minerals. Geochim. Cosmochim. Acta 57, 1079–1091.

Zheng, Y.F., 1993b. Calculation of oxygen isotope fractionation in hydroxyl-bearing silicates. Earth Planet. Sci. Lett. 120, 247–263.

Zheng, Y.F., Fu, B., 1998. Estimation of oxygen diffusivity from anion porosity in minerals. Geochem. J. 32, 71–89.

Zheng, Y.F., Wang, Z.R., Li, S.G., Zhao, Z.F., 2002. Oxygen isotope equilibrium between eclogite minerals and its constraints on mineral Sm–Nd chronometer. Geochim. Cosmochim. Acta 66, 625–634.

Zheng, Y.F., Fu, B., Gong, B., Li, L., 2003. Stable isotope geochemistry of ultrahigh pressure metamorphic rocks from the Dabie–Sulu orogen in China: implications for geodynamics and fluid regime. Earth Sci. Rev. 62, 105–161.

Zheng, Y.F., Wu, Y.B., Chen, F.K., Gong, B., Li, L., Zhao, Z.F., 2004. Zircon U–Pb and oxygen isotope evidence for a large-scale ^{18}O depletion event in igneous rocks during the Neoproterozoic. Geochim. Cosmochim. Acta 68, 4145–4165.

Zheng, Y.-F., Wu, Y.-B., Zhao, Z.-F., Zhang, S.-B., Xu, P., Wu, F.-Y., 2005a. Metamorphic effect on zircon Lu–Hf and U–Pb isotope systems in ultrahigh-pressure eclogite-facies metagranite and metabasite. Earth Planet. Sci. Lett. 240, 378–400.

Zheng, Y.-F., Zhou, J.-B., Wu, Y.-B., Xie, Z., 2005b. Low-grade metamorphic rocks in the Dabie–Sulu orogenic belt: a passive-margin accretionary wedge deformed during continent subduction. Intern. Geol. Rev. 47, 851–871.

Zheng, Y.-F., Zhao, Z.-F., Wu, Y.-B., Zhang, S.-B., Liu, X.M., Wu, F.-Y., 2006. Zircon U–Pb age, Hf and O isotope constraints on protolith origin of ultrahigh-pressure eclogite and gneiss in the Dabie orogen. Chem. Geol. 231, 135–138.

Zheng, Y.-F., Zhang, S.-B., Zhao, Z.-F., Wu, Y.-B., Li, X., Li, Z., Wu, F.-Y., 2007a. Contrasting zircon Hf and O isotopes in the two episodes of Neoproterozoic granitoids in South China: implications for growth and reworking of continental crust. Lithos 96, 127–150.

Zheng, Y.-F., Wu, Y.-B., Gong, B., Chen, R.-X, Tang, J., Zhao, Z.-F., 2007b. Tectonic driving of Neoproterozoic glaciations: evidence from extreme oxygen isotope signature of meteoric water in granite. Earth Planet. Sci. Lett. 256, 196–210.

Zhou, M.-F., Zhao, T.-P., Malpas, J., Sun, M., 2000. Crustal-contaminated komatiitic basalts in Southern China: products of a Proterozoic mantle plume beneath the Yangtze Block. Precambr. Res. 103, 175–189.

Zhou, M.-F., Yan, D.-P., Kennedy, A.K., Li, Y.-Q., Ding, J., 2002a. SHRIMP U–Pb zircon geochronological and geochemical evidence for Neoproterozoic arc-magmatism along the western margin of the Yangtze Block, South China. Earth Planet. Sci. Lett. 196, 51–67.

Zhou, M.-F., Kennedy, A.K., Sun, M., Maipas, J., Lesher, C.M., 2002b. Neoproterozoic arc-related mafic intrusions along the northern margin of South China: implications for the accretion of Rodinia. J. Geol. 110, 611–618.

Zhou, J.C., Wang, X.L., Qiu, J.S., Gao, J.F., 2004. Geochemistry of Meso- and Neoproterozoic mafic-ultramafic rocks from northern Guangxi, China: arc or plume magmatism? Geochem. J. 38, 139–152.

Zhou, M.F., Ma, Y.X., Yan, D.P., Xia, X.P., Zhao, J.H., Sun, M., 2006a. The Yanbian terrane (Southern Sichuan Province, SW China): a Neoproterozoic arc assemblage in the western margin of the Yangtze block. Precambr. Res. 144, 19–38.

Zhou, M.-F., Yan, D.-P., Wang, C.-L., Qi, L., Kennedy, A., 2006b. Subduction-related origin of the 750 Ma Xuelongbao adakitic complex (Sichuan Province, China): implications for the tectonic setting of the giant Neoproterozoic magmatic event in South China. Earth Planet. Sci. Lett. 248, 286–300.

Zhou, J.B., Li, X.-H., Ge, W.C., Li, Z.-X., 2007a. Age and origin of middle Neoproterozoic mafic magmatism in southern Yangtze Block and relevance to the break-up of Rodinia. Gondwana Res. 12, 184–197.

Zhou, M.-F., Zhao, J.-H., Xia, X.P., Sun, W.-H., Yan, D.-P., 2007b. Comment on "Revisiting the "Yanbian Terrane": Implications for Neoproterozoic tectonic evolution of the western Yangtze Block, South China" [Precambr. Res. 151 (2006) 14–30]. Precambr. Res. 155, 313–317.

Zhu, W.-G., Zhong, H., Deng, H.-L., Wilson, A.H., Liu, B.-G., Li, C.-Y., Qin, Y., 2006. SHRIMP zircon U–Pb age, geochemistry, and Nd–Sr isotopes of the Gaojiacun mafic-ultramafic intrusive complex, Southwest China. Intern. Geol. Rev. 48, 650–668.